Remote Sensing of Environment xxx (xxxx) xxx

Contents lists available at ScienceDirect

Remote Sensing of Environment

journal homepage: www.elsevier.com/locate/rse

Quality-control tests for OC4, OC5 and NIR-red satellite chlorophyll-a algorithms applied to coastal waters

H. Lavigne [a,*], D. Van der Zande [a], K. Ruddick [a], J.F. Cardoso Dos Santos [a], F. Gohin [b], V. Brotas [c], S. Kratzer [d]

[a] Royal Belgium Institute of Natural Sciences (RBINS), Operational Directorate Natural Environment, 29 Rue Vautierstraat, 1000 Brussels, Belgium
[b] IFREMER, DYNECO PELAGOS, CS 10070, 29280 Plouzané, France
[c] Marine Environmental Sciences Centre, Faculdade de Ciências, Universidade de Lisboa, Campo Grande 1749-016, Lisboa, Portugal
[d] Department of Ecology, Environment and Plant Sciences, Stockholm University, 10691 Stockholm, Sweden

ARTICLE INFO

Keywords:
Ocean colour
Chlorophyll-a algorithms
Coastal waters
Quality control
Algorithm-switching approach
MERIS
OLCI
Sentinel-3

ABSTRACT

Reliable satellite estimates of chlorophyll-a concentration (Chl-a) are needed in coastal waters for applications such as eutrophication monitoring. However, because of the optical complexity of coastal waters, retrieving accurate Chl-a is still challenging. Many algorithms exist and give quite different performance for different optical conditions but there is no clear definition of the limits of applicability of each algorithm and no clear basis for deciding which algorithm to apply to any given image pixel (reflectance spectrum). Poor quality satellite Chl-a data can easily reach end-users. To remedy this and provide a clear decision on when a specific Chl-a algorithm can be used, we propose simple quality control tests, based on MERIS water leaving reflectance (ρ_w) bands, to determine on a pixel-by-pixel basis if any of three popular and complementary algorithms can be used. The algorithms being tested are: 1. the OC4 blue-green band ratio algorithm which was designed for open ocean waters; 2. the OC5 algorithm which is based on look-up tables and corrects OC4 overestimation in moderately turbid waters and 3. a near infrared-red (NIR-red) band ratio algorithm designed for eutrophic waters.

Using a dataset of 348 in situ Chl-a / MERIS matchups, the conditions for reliable performance of each of the selected algorithms are determined. The approach proposed here looks for the best compromise between the minimization of the relative difference between In situ measurements and satellite estimations and the number of pixels processed. Conditions for a reliable application of OC4 and OC5 depend on ρ_w412/ρ_w443 and ρ_w560, used as proxies of coloured dissolved organic matter and suspended particulate matter (SPM), as compared to ρ_w560/ρ_w490, used as a proxy for Chl-a. Conditions for reliable application of the NIR-red band ratio algorithm depend on Chl-a and SPM. These conditions are translated into pixel-based quality control (QC) tests with appropriately chosen thresholds. Results show that by removing data which do not pass QC, the performance of the three selected algorithms is significantly improved. After combining these algorithms, 70% of the dataset could be processed with a median absolute percent difference of 30.5%. The QC tests and algorithm merging methodology were then tested on four MERIS images of European waters. The OC5 algorithm was found to be suitable for most pixels, except in very turbid and eutrophic waters along the coasts where the NIR-red band ratio algorithm helps to fill the gap. Finally, a test was performed on an OLCI-S3A image. Although some validations of water reflectance are still needed for the OLCI sensors, results show similar behavior to the MERIS applications which suggests that when applied to OLCI data the present methodology will help to accurately estimate Chl-a in coastal waters for the next decade.

1. Introduction

Chlorophyll-a concentration (Chl-a hereafter), a proxy for phytoplankton biomass, is needed for a variety of applications in coastal waters, including fish-farming (Gernez et al., 2017; Chassot et al., 2010), and eutrophication monitoring (Reinart and Kutser, 2006; Harvey et al., 2015). In particular, there is a growing interest in the use of satellite Chl-a data for eutrophication monitoring (European Commission, 2014;

* Corresponding author.
E-mail address: hlavigne@naturalsciences.be (H. Lavigne).

https://doi.org/10.1016/j.rse.2020.112237
Received 30 March 2020; Received in revised form 27 October 2020; Accepted 1 December 2020

OSPAR, 2017; Gohin et al., 2019) in the context of legal obligations on EU member states under the Water Framework Directive (WFD) and Marine Strategy Framework Directive (MSFD). Indeed, contrary to in situ data, satellite data allows for more coherent transnational approaches within and between marine regions and sub-regions.

There has been considerable success in retrieving accurate Chl-a from water reflectance with blue/green-ratio algorithms such as OC4 (O'Reilly et al., 1998) in oceanic "case 1" waters (Morel and Prieur, 1977) where the variation of optical in-water properties (absorption and scattering) is dominated by phytoplankton and associated material. In contrast, the optical complexity of coastal waters makes it difficult to accurately retrieve biogeochemical parameters using satellite remote sensing (Sathyendranath et al., 1989; Lee and Hu, 2006; Dierssen, 2010). Chl-a retrieval by blue/green band-ratio algorithms tends to fail when applied to coastal waters where optical properties may be strongly influenced by non-covarying concentrations of suspended particulate matter (SPM) and coloured dissolved organic matter (CDOM) or where the Chl-a can reach extremely high values (Smith, 2003; Goyer et al., 2005; Smith et al., 2018). Such waters are defined as optical "case 2" waters, and a large variety of regional algorithms have been developed to improve Chl-a estimations from water reflectance in these types of waters (see Odermatt et al., 2012 for a review). However, there is in general no clear definition of when an algorithm will give reliable output nor of which algorithm will perform best for each image pixel. This lack of knowledge on validity domains of algorithms also prevents any automatic and reliable global processing.

In order to tackle this problem and facilitate automated processing for any water type, we define a set of simple "quality control tests" (QC tests hereafter) for three popular and complementary Chl-a algorithms. These QC tests first define a validity domain for each algorithm and ensure the validity of a Chl-a estimate within a certain uncertainty range. They also allow to switch between Chl-a algorithms when they are used in a complementary way. The selected Chl-a algorithms are the classic empirical blue-green bands ratio algorithm (OC4, O'Reilly et al., 1998), the five channel Chl-a algorithm for coastal water (Gohin et al., 2002, named OC5 hereafter) and finally the semi-analytic near infrared (NIR) - red band ratio algorithm defined by Gons (1999). OC4 is an empirical blue-green band ratio algorithm with the shortest spectral band shifting from 443 nm to 510 nm with increasing Chl-a. This algorithm is designed for case 1 waters and its median error was estimated to be around 35% for oceanic waters at global scale (Bailey and Werdell, 2006). Although OC4 is generally not suitable for coastal waters where it often overestimates the Chl-a concentration because of high CDOM absorption and/or SPM concentration (Dierssen, 2010), it can be used for certain coastal zones with optical water properties close to those of the open ocean. The OC5 algorithm is an empirical algorithm based on look up tables (LUTs). It has been designed to correct the overestimation of the OC4 algorithm in moderately turbid and/or high CDOM waters and is based on a training dataset from the western Mediterranean Sea, the Bay of Biscay and the English Channel. OC5 LUTs are based on a triplet of entries: the maximum ratio of reflectance blue/green used by the OC4 algorithm and the normalized water leaving radiances at 412 and at 560 nm. The OC5 LUTs were originally developed for the SeaWiFS sensors (Gohin et al., 2002) but additional LUTs adapted to other ocean colour sensors (MODIS AQUA, MERIS and OLCI) are available. The third algorithm evaluated in this study is the Gons (1999) algorithm. It is based on the NIR-red band ratio (i.e. reflectance bands 705 nm and 665 nm) which increases with Chl-a. These types of algorithms are applicable in turbid, eutrophic waters where the NIR-red reflectance is significant enough to be insensitive to radiometric noise and where the effect of red Chl-a absorption is sufficient to be measurable. Among the variety of NIR-red band ratio algorithms (Dall'Olmo et al., 2005; Gitelson et al., 2007; Le et al., 2009; Moses et al., 2009; Gilerson et al., 2010), we selected the Gons (1999) version because of its semi-analytical structure which makes it less dependent on validation datasets compared to empirical algorithms. However, this algorithm is based on some assumptions and a final calibration step. In fact, the Gons (1999) algorithm assumes a constant back scattering coefficient in the red and NIR, a negligible absorption from CDOM and non-algal particles compared to water absorption at 672 nm, 704 nm and 750 nm and to water and chlorophyll-a absorption at 672 nm. Finally, a constant chlorophyll-a specific absorption coefficient is assumed.

Previously, application criteria based on remote sensing reflectances (Lee and Hu, 2006; Morel and Bélanger, 2006; Park et al., 2010) or parameters such as Chl-a itself (Bricaud and Morel, 1987) have been proposed to identify case 1 waters where OC4 can be readily applied. The criteria proposed by Lee and Hu (2006) are based on the average relationship (observed at global scale) between Chl-a and suspended particulate matter concentration on the one hand and between the Chl-a concentration and CDOM absorption on the other hand, which allows to distinguish case 1 from case 2 waters. With an approach based on simulations using a model for inherent optical properties, Park et al. (2010) provided a quality control flag for the utilization of MODIS Chl-a estimations derived from the OC4 algorithm in turbid waters. Assuming that the single case-1/case-2 waters differentiation is not sufficient to describe the diversity of optical water characteristics, Moore et al. (2001) described 6 optical water types derived from clustering analysis applied to reflectance spectra. Then, for any satellite reflectance spectra, a membership index to each optical water type is calculated allowing the selection and blending of bio-optical algorithms. Based on this methodology, uncertainty products for MODIS Chl-a were calculated (Moore et al., 2009). Using a similar methodology, Hieronymi et al. (2017) blended 13 Chl-a neural network algorithms developed for 13 optical water classes in order to process waters ranging from extremely turbid to extremely absorbing (high CDOM) and Jackson et al. (2017) presented a new set of 14 optical water classes that result from the OC-CCI implementation of the Moore et al. (2009) fuzzy classification approach. Recently, Neil et al. (2019) tested 48 Chl-a algorithms on a dataset covering the 13 optical water types and attempted to provide recommendations for each water type. Nevertheless, as the same reflectance spectra may result from a large diversity of water constituent combinations (Hieronymi et al., 2017) with different absorbing and scattering properties, Chl-a retrieval within the same optical water class can sometimes be rather challenging. To process oligotrophic and eutrophic waters simultaneously, alternative switching algorithms using blue-green and NIR-red band-ratio algorithms have been proposed (Gons et al., 2008; Smith et al., 2018) but they have been developed/tested for certain regions and water types (i.e. case 1 waters in Smith et al., 2018). Given the large variety of coastal and inland waters and Chl-a algorithms presenting different degrees of complexity, the user can easily be confused when it comes to selecting an appropriate Chl-a algorithm. A given algorithm may be derived from a limited regional or local data set or even from a synthetic database, and it is not easy to know which algorithms works best in the coastal area that one wants to investigate.

The aim of this study is to develop and to provide robust reflectance-based QC tests and a suitable algorithm switching approach for coastal waters in order to choose between OC4, OC5 and Gons (1999) algorithms. QC tests should avoid unreliable algorithm performances whereas the switching approach reduces the overall uncertainties while processing most of the pixels. QC tests are developed with a novel methodology based on percent difference of satellite estimations compared to the respective in situ match-up data.

An in situ/satellite matchups dataset was produced using water reflectance from the MEdium Resolution Imaging Spectrometer (MERIS; Rast et al., 1999). The MERIS sensor was selected for the analysis because of its long operational period (from March 2002 to May 2012), which over the years has allowed ESA's MERIS validation team to collect a reasonable number of in situ/satellite reflectance match-up data, covering different water types. ESA have recently launched the Sentinel-3 series of follow-up missions for MERIS, each hosting an Ocean and Land Colour Instrument (OLCI, Nieke et al., 2012) with spectral characteristics are very close to MERIS. In addition, the 709 nm band,

present on MERIS and OLCI (but not available for MODIS and VIIRS), is particularly useful for Chl-a estimation in turbid, eutrophic waters. The following sections describe the datasets used and the methodology to determine reflectance-based quality control tests for the OC4, OC5 and NIR-Red band ratio algorithms. In the results section, we present the derivation of these QC tests, the performance of the algorithms before and after QC, as well as examples of applications to MERIS and OLCI data. Finally, this novel methodology for the design and application of QC tests as well as the approach used for switching between algorithms is discussed and potential applications in support of the European Marine Strategy Directive (MFSD) are presented.

2. Data and methods

2.1. Chl-a in situ/satellite matchups

A total of 235 in situ Chl-a and MERIS matchups were extracted from the MERMAID database (http://mermaid.acri.fr/home/home.php, Barker et al., 2008) with MEGS 8.1 processing at reduced resolution (RR, spatial resolution: 1040 m × 1160 m). In situ Chl-a was mostly determined with High Performance Liquid Chromatography (HPLC, 95%) otherwise with spectrophotometry (5%). The Chl-a in situ database was complemented with measurements published in the Coast Colour Round Robin (CCRR) dataset (Nechad et al., 2015) providing in situ optical and biogeochemical data from different coastal regions over the world. In the CCRR dataset, Chl-a was measured by lab fluorometry (57%) and HPLC (43%). Fluorometry measurements were performed after water filtration and extraction in solvent, detailed protocols are provided in Nechad et al., 2015. MERIS match-ups were extracted from MEGS8.1 RR level 2 products downloaded from the ODESA platform (http://www.odesa-info.eu/info/) for the CCRR in situ Chl-a observations. Reduced resolution is provided by the MERMAID platform for matchups extraction and was used by the MERIS validation team (Barker et al., 2008). For the MERMAID and CCRR datasets, MERIS matchups were acquired in a time window of ±2.5 h from the in situ observation. The median of nine pixels around the location of the in situ measurement was used (macropixels). Data was accepted if at least 3/9 valid pixels were available in the respective macropixel, and if no extreme variation was observed in a micropixel (coefficient of variation lower than 1.5). The following Level-2 data quality masks were applied to the MEGS 8.1 water leaving reflectance (ρ_w hereafter) data: LAND, CLOUD, HIGH_GLINT, MEDIUM_GLINT, and LOW_SUN. A final quality control step was applied to remove data points with negative ρ_w values at 443 nm. No additional quality control was applied to in situ Chl-a data as the validity and consistency of the data were previously verified by the contributors and managers of the CCRR and MERMAID database (Nechad et al., 2015; Barker et al., 2008). The resulting dataset (Table 1) contained 348 Chl-a/MERIS matchups from July 2002 to July 2011, with 235 points from the MERMAID dataset and 113 points from the CCRR dataset with in situ Chl-a ranging from 0.05 mg per cubic meter (mg m^{-3}) to 31 mg m^{-3}. Data points are mostly distributed in North European waters and to a lesser extent along North America coasts (Fig. 1) but cover a wide variety of optical conditions.

Chl-a products were generated using MERIS-dedicated algorithms. The OC4 blue-green band ratio algorithm was computed with factors recently updated by O'Reilly and Werdell (2019). The MERIS adaptation proposed by Gons et al. (2002) and Gons et al. (2005) was used for updating the NIR-red band ratio algorithm of Gons (1999). A LUT specific to the spectral reflectance of MERIS processed by MEGS8.1 was used to retrieve OC5 Chl-a (Gohin et al., 2002; Gohin, 2011). Detailed information on these algorithms can be found in Table 2. In the following, these algorithms will be referred to as OC4, OC5 and NIR-RED with their respective Chl-a products CHL_OC4, CHL_OC5 and CHL_RED. Fig. 2 shows scatterplots of in situ Chl-a versus CHL_OC4, CHL_OC5 and CHL_RED in logarithmic (panels A, B and C) and linear scales (panels D, E and F). Scatterplots show expected patterns (see Section 3.2 for a detailed discussion) with an overestimation of CHL_OC4 and to a lesser extent CHL_OC5. A high scatter of CHL_RED when in situ Chl-a is low is also observed. This is not surprising as NIR_RED algorithm is known to be applicable only for eutrophic waters (Gons et al., 2002). Finally, no impact of the data source (HPLC, fluorometry and spectrophotometry) on the quality of the matchup can be observed suggesting a good coherence of the dataset.

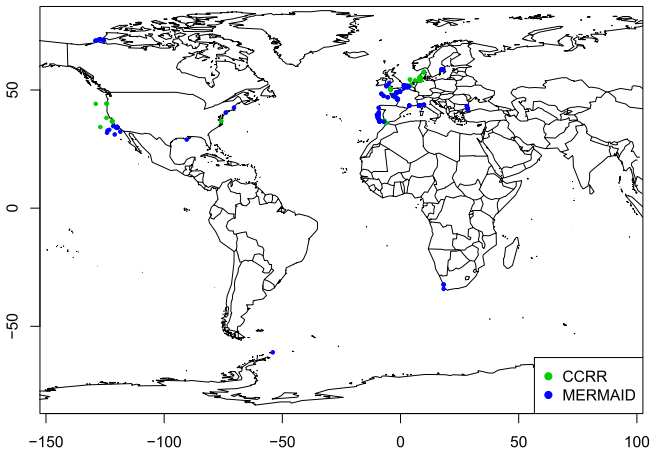

Fig. 1. Spatial distribution of the in situ Chl-a observations with a MERIS matchup in the CCRR-MERMAID dataset. The highest number of observations was measured in the North Sea.

Table 1
Description of the CCRR-MERMAID database.

Database	Region (code)	Chl-a measurement	Chl-a range (mg m-3)	Number of matchups
CCRR	Central California	fluorometry	1.09–11.28	6
CCRR	Southern California	HPLC	0.10–6.03	9
CCRR	Chesapeake Bay	HPLC	9.3–12.3	3
CCRR	Med. Sea (Morocco)	fluorometry	0.12–1.62	12
CCRR	North Sea	fluorometry	0.30–31.5	39
CCRR	North Sea	HPLC	0.53–8.65	41
CCRR	Oregon Washington	HPLC	0.20–0.84	3
MERMAID	Atlantic coast of Portugal (Algarve / PortCoast)	HPLC	0.11–3.08	59
MERMAID	Black Sea (BioOptEuroFleets)	HPLC	0.34–0.62	5
MERMAID	North-Western Med. Sea (Boussole)	HPLC	0.07–3.16	21
MERMAID	Bristol Irish Sea (Bristol Channel and Irish Sea)	Spectrophotometry	0.45–0.92	4
MERMAID	Beaufort Sea (CASES)	HPLC	0.23–3.52	8
MERMAID	North Sea (MUMMTriOS)	HPLC	0.33–27.28	33
MERMAID	Baltic Sea (N.W. Baltic Sea)	Spectrophotometry	1.09–6.27	10
MERMAID	Southern California (PlumesAndBlooms)	HPLC	0.38–4.97	36
MERMAID	French coastal waters (REPHY)	HPLC	0.40–31.5	59

Table 2
Description of the three Chl-a algorithms considered in this study.

Algorithm	Reference	Description
OC4	O'Reilly and Werdell (2019)	$Chla = 10^{(a+bR+cR^2+dR^3+eR^4)}$ where $R = log_{10}\left(max\left(\frac{\rho_w 443}{\rho_w 560}, \frac{\rho_w 490}{\rho_w 560}, \frac{\rho_w 510}{\rho_w 560}\right)\right)$ $a = 0.42487$, $b = -3.20974$, $c = 2.89721$, d = −075258, e = −0.98259
OC5	Gohin et al. (2002)	Chla is a function of CHL_OC4, $\rho_w 412$ and $\rho_w 560$. Specific OC5 LUTS for MERIS were provided by F. Gohin.
NIR-RED	Gons et al. (2005)	$Chla = \frac{1}{0.0161} \cdot \frac{\rho_w 709}{\rho_w 665} \cdot (0.70 + b_b) - 0.40 - b_b^{1.062}$ $b_b = \frac{1.61 \cdot \rho_w 779}{(0.082 - 0.6 \cdot \rho_w 779)}$

2.2. Assessment of satellite Chl-a algorithm performance

Following the recommendations of Bailey and Werdell (2006) satellite Chl-a estimations were assessed against in situ data with the metrics listed below:

- The median ratio (MR hereafter) is defined as

$$MR = median\left(\frac{Chl - a_{sat}}{Chl - a_{situ}}\right) \quad (1)$$

This metric allows to measure a potential bias in the Chl-a estimation. If satellite estimations overestimate Chl-a concentration MR is significantly higher than 1, if Chl-a concentrations are underestimated MR is significantly lower than 1.

- The median absolute percent difference (MAPD) indicates the relative difference between in situ observation and satellite estimation and is computed via

$$MAPD = median\left(100 \times \frac{|Chla_{sat} - Chla_{situ}|}{Chla_{situ}}\right) \quad (2)$$

A type 1 linear regression is also computed between Chl-a_{sat} and Chl-$a_{in\ situ}$ and the following metrics were considered:

- The Root Mean Square of Difference (RMSD), which measures the scatter of the data from the regression line.
- The slope and the intercept of the regression line allow to see if there is a systematic multiplicative or additive bias
- The coefficient of determination (r^2) measures the goodness of fit of the linear regression for satellite Chl-a retrieval as function of the in situ Chl-a and depends strongly on the dataset range.

2.3. Definition of application criteria

2.3.1. Methodology overview

Fig. 3 provides a general overview of the approach used to determine the algorithm-specific application criteria. Starting from a priori knowledge on the OC4, OC5 and NIR-RED algorithms, a set of conditions for the optimal performance of each algorithm was defined and

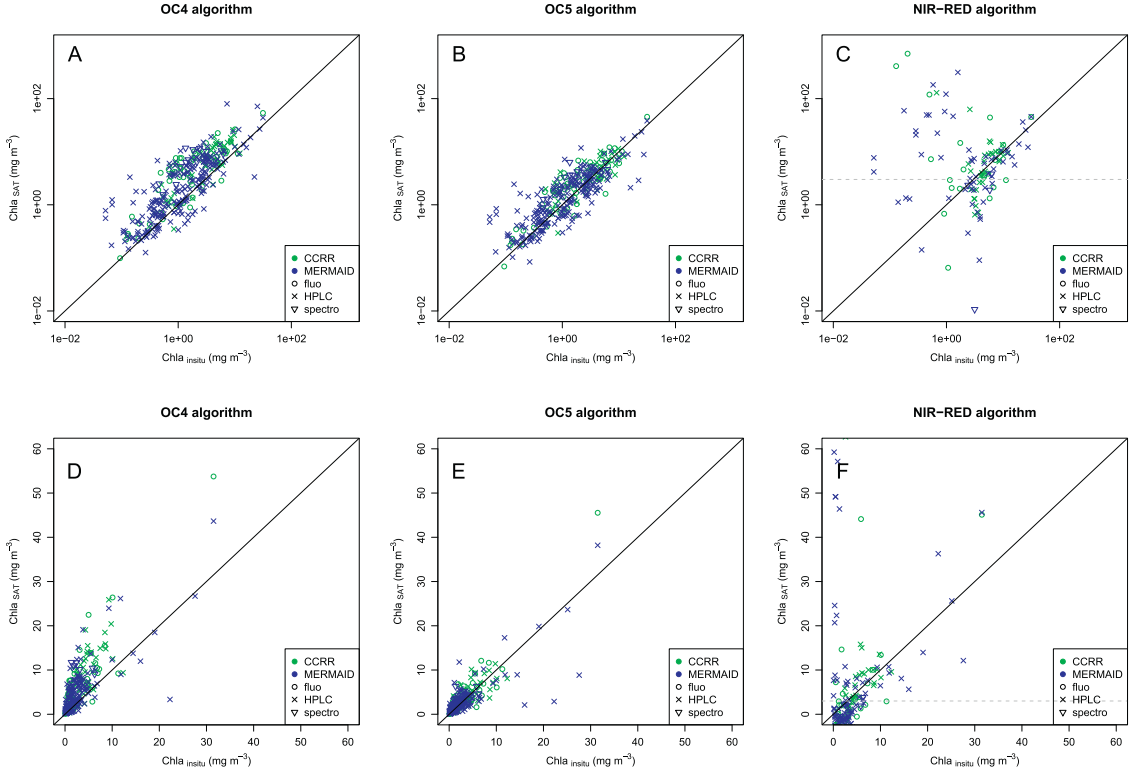

Fig. 2. Chl-a estimated from MERIS reflectance with OC4 (panels A and D), OC5 (panels B and E) and NIR-RED (panels C and F) algorithms, compared to in situ Chl-a. For a better visualisation scatterplots are presented in log-log (upper panels) and linear-linear scale (lower panels). For the NIR-RED algorithm (right panels), the dotted grey line represents the limit Chl-a = 3 mg m^{-3} that it is recommended to consider when applying this algorithm. Performance metrics for these algorithms applied to the whole CCRR-MERMAID dataset are given in Table 4 (Lines 1 to 3).

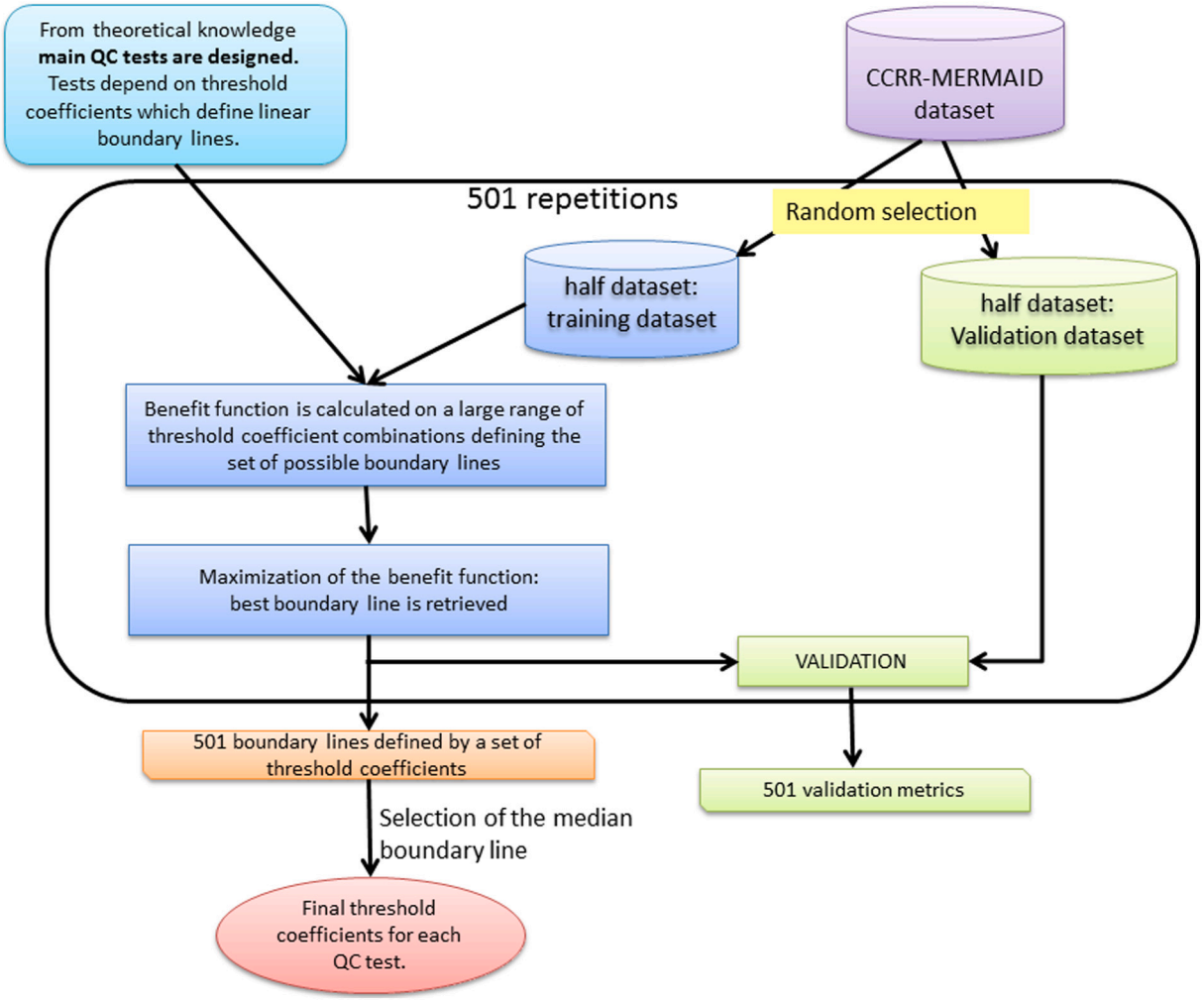

Fig. 3. Flow chart showing the general methodology used to define all QC tests including the validation on an independent data set.

translated to algorithm specific QC tests. The QC tests consisted of different band and band-ratio thresholds. These thresholds are represented by linear lines (hereafter "boundary lines") which are defined with slope and intercept coefficients (hereafter, "threshold coefficients"). The determination of these threshold coefficients was based on the CCRR-MERMAID dataset. This dataset was divided into two equally large, but randomly selected subsets for the determination of the threshold coefficients on one side and their validation on the other side. The dataset division was repeated 501 times to ensure the robustness of the results. This number of repetitions has been chosen to ensure that most of the splitting combinations are represented while keeping a reasonably short processing time and the odd number facilitate the extraction of the median boundary lines. For each division the optimal threshold coefficients were determined using an objective benefit function approach based on the relative percent difference between in situ and satellite-based Chl-a for each element in the training dataset. From the 501 boundary lines obtained for each division, the line with the median position was selected as the final boundary line defining the algorithm QC test.

2.3.2. *Model definition*

The Chl-a algorithms under consideration (i.e. OC4, OC5 and NIR-RED) usually only apply to specific optical water types. Lee and Hu (2006) provided criteria for the determination of case 1 waters based on ρ_w with the following principles: (1) ρ_w can provide proxies for CDOM absorption, concentration of Chl-a and SPM and (2) CDOM absorption and SPM concentrations are each a function of the Chl-a concentration. For these waters, the Chl-a concentration can be approximated with the green – blue band ratio (ρ_w560/ρ_w490, named R53 hereafter), the SPM concentration with the reflectance at 560 nm (ρ_w560, named R5 hereafter) and CDOM absorption is inversely related to the band ratio ρ_w412/ρ_w443 (named R12 hereafter). In case 1 waters, R12 and R5 are functions of R53. The average case 1 water is defined by the relationship between R12 and R53 and between R5 and R53. Considering all pixels of the global ocean, Lee and Hu (2006) proposed models of R12 and R5 as 3-degree polynomial functions of R53. Pixels deviating by more than 10% from the average model were considered as case 2 waters. Most of the case 2 pixels could be explained by high CDOM compared to Chl-a with points situated below the −10% limit of R12 predicted from R53 and/or by high SPM compared to Chl-a concentration with points situated above the +10% limit of R5 predicted from R53 (Lee and Hu, 2006).

To determine for which conditions of high SPM and CDOM the OC4 and OC5 algorithms can provide reliable Chl-a estimates, we adopted a similar approach to Lee and Hu (2006) and constrained the application of OC4 and OC5 algorithms to restrictive conditions on R12 and $\log_{10}$(R5) as function of R53. Then, OC4 and OC5 algorithms apply if R12 is higher than a certain threshold defined by a boundary line and if $\log_{10}$(R5) is lower than another boundary line. Hence, two boundary lines have to be defined. These lines are function of R53 and represent the increase with Chl-a of CDOM and SPM content in case 1 waters. The logarithmic transformation was used on the reflectance (i.e. $\log_{10}$(R5)),

but not on reflectance ratios, to make the data distribution more homoscedastic. QC tests for the OC4 and OC5 algorithms are defined according to the following equations:

$$\text{Main QC tests OC4} \begin{cases} R12 \geq L_{R12_{OC4}}(R53) \\ with\ L_{R12_{OC4}}(R53) = i_{R12_{OC4}} + s_{R12_{OC4}}\ R53 \\ log_{10}(R5) \leq L_{logR5_{OC4}}(R53) \\ with\ L_{logR5_{OC4}} = i_{logR5_{OC4}} + s_{logR5_{OC4}}\ R53 \end{cases} \quad (3)$$

$$\text{Main QC tests OC5} \begin{cases} R12 \geq L_{R12_{OC5}}(R53) \\ with\ L_{R12_{OC5}}(R53) = i_{R12_{OC4}} + s_{R12_{OC5}}\ R53 \\ log_{10}(R5) \leq L_{logR5_{OC5}}(R53) \\ with\ L_{logR5_{OC5}} = i_{logR5_{OC4}} + s_{logR5_{OC5}}\ R53 \end{cases} \quad (4)$$

In Eqs. (3) and (4) parameters i and s are intercept and slope coefficients of the boundary lines. The calculation of these parameters is detailed in Section 3.1.

The NIR-RED algorithm is based on Chl-a absorption in the red spectral band. In clear waters the NIR water reflectance is very low and the NIR-red band ratio is strongly affected by radiometric noise and/or atmospheric correction errors giving very scattered and erroneous Chl-a estimates (see Fig. 2, panel C and Ruddick et al., 2001, Fig. 5). Additionally, in turbid waters with low Chl-a concentrations the impact of Chl-a absorption on the red reflectance may not be detectable (Gitelson, 1992; Ruddick et al., 2001; Gons et al., 2008). Hence, the application criteria for the NIR-RED algorithm are based on both the Chl-a concentration and reflectance in the NIR bands. Since for low to moderate Chl-a concentrations, the OC4 algorithm is more reliable than the NIR-RED algorithm (compare Fig. 2 panels A and C), CHL_OC4 was used as a proxy of Chl-a concentration here. Because the 665 nm band is affected by Chl-a absorption, water reflectance at 620 nm (ρ_w620, R6 hereafter) is used as an index for water reflectance in the red. Thus, the main QC tests for the NIR-RED algorithm are expressed as:

$$Main\ QC\ tests\ NIR-RED \begin{cases} CHL\_OC4 \geq L_{Chl/NIR\_RED} \\ R6 \geq L_{R6/NIR\_RED} \end{cases} \quad (5)$$

where L_{Chl/NIR_RED} and L_{R6/NIR_RED} are constant values representing respectively the minimum CHL_OC4 and R6 values to apply the NIR-RED algorithm.

2.3.3. Determination of threshold coefficients

In order to parameterize and validate the QC tests with two independent datasets, the initial CCRR-MERMAID dataset consisting of 348 data points was randomly divided into two datasets of 174 data points, named training and validation dataset respectively. Then, using the training dataset, threshold coefficients for boundary lines (i.e. L_{R12_OC4}, L_{logR5_OC4}, L_{R12_OC5}, L_{logR5_OC5}, L_{Chl/NIR_RED} and L_{R6/NIR_RED}) were determined.

To obtain optimal and objectives values, a benefit function (*BF*) was defined as:

$$BF = \sum_i y_i \text{ with } \begin{cases} y_i = +5\ if\ APD_i \leq 30 \\ y_i = +2\ if\ 30 < APD_i \leq 50 \\ y_i = -2\ if\ 50 < APD_i \leq 100 \\ y_i = -5\ if\ APD_i > 100 \end{cases} \quad (6)$$

where i stands for any points passing QC tests for OC4, OC5 or NIR-RED models and APD is the absolute percent difference and is defined as.

$$APD = 100\left|\frac{Chla_{sat} - Chla_{situ}}{Chla_{situ}}\right| \quad (7)$$

BF increases when the number of low ADP matchups (APD < 50%) passing the QC increases and decreases when the number of high ADP matchups passing QC (APD > 50%) increases. By attempting to maximize the *BF*, one identifies the best compromise between including the largest number of low APD matchups in the selection while avoiding high APD matchups. For each training set, *BF* was computed for a large range of threshold coefficients in order to test all the potential boundary lines and retain the best one. The range of threshold coefficients tested is given in Table 3 (numbers in brackets) and is motivated in Section 3.1. To achieve a robust choice of the best thresholds the random division of the whole dataset was repeated 501 times – each of the 501 training sets gives the threshold coefficients which optimize the BF and, applied to the validation subset, it provides different results for the validation metrics. Threshold coefficients come by pairs (slope and intercept) for defining OC4 and OC5 boundary lines whereas they are single values defining horizontal/vertical boundary lines for the NIR-red algorithm. In case of single threshold coefficients, the median is used to define the final threshold coefficient value. In case of pairs (i.e. slope and intercept), among the 501 boundary lines obtained, the one with the median position is selected and its slope and intercept values defined the final threshold coefficients. The median position is defined by the position of the line for which the area under the curve for R53 ranging between 0.5 and 2.5 has a median value.

3. Results

3.1. QC tests for OC4, OC5 and NIR-RED algorithm

3.1.1. QC test for OC4 algorithm

Fig. 4 shows how the distribution of R12, which is a proxy for CDOM, is inversely related to R53, a proxy of Chl-a (panel A) and how $\log_{10}$(R5), a proxy of SPM, is positively correlated to R53 (panel B). For each point, the relative in situ/satellite difference (APD Eq. (7)) is indicated with a colour code. The results show that low R12 and high $\log_{10}$(R5) values at constant R53 tend to be associated with an overestimation of Chl-a by the OC4 algorithm (red and orange points). This result is consistent with previous findings (Moore et al., 2009; Dierssen, 2010) which demonstrated an overestimation of Chl-a by the OC4 algorithm in the case of high CDOM and/or SPM. Considering the data distribution displayed in Fig. 4, it was decided to impose some restrictions on the range of tested threshold coefficients (see Table 2 numbers in brackets) when calculating the benefit function BF so that the boundary lines which are tested roughly follow the main trend in data distribution. Thus, a negative slope is expected for the high CDOM test and a positive slope is expected for the high SPM test. In addition, the intercept has been constrained to the R12 or $\log_{10}$(R5) range of values corresponding to the points showing the lowest R53 signal (in practice the first decile was selected). Then, for the high CDOM test (R12 as a function of R53), the benefit function was calculated for intercept values ranging between 0.79 and 1.14 and the slope values between 0 and −3 by increments of 0.01. For the high SPM test ($\log_{10}$(R5) as a function of R53), BF was calculated for intercept values ranging between −2.51 and −2.15 and slope between 0 and 5 by increments of 0.01. For 20 iterations out of the 501, boundary lines maximizing BF are represented with grey dotted lines on Fig. 4 and the final boundary line which is the median of the 501 iterations is represented by the solid black line on each panel of Fig. 4. Definitive threshold coefficients are given in Table 2. For both tests, the threshold lines separate well areas dominated with low percent difference points (yellow, green and clear blue points) from the areas with a majority of very high percent difference matchups (red points). However, the scatterplot of R12 as a function of R53 (Fig. 4A) shows that data with a high R12 band ratio (R12 > 1.25) give severe underestimations of Chl-a by OC4 algorithms (blue points). This is most likely due to a failure of the atmospheric correction algorithm or factors such as sun glint affecting the quality of remote sensing data as it is expected that the maximum R12 (minimum CDOM) is observed in case 1 waters. Hence, data points with a R12 band ratio higher than 1.25 were flagged as "possible atmospheric correction error". In addition to these previous tests, a limit range for Chl-a values was also introduced (Lee and Hu, 2006). Indeed, OC4 and OC5 algorithms apply only for oligotrophic and mesotrophic waters (Odermatt et al., 2012; Matsushita et al., 2015; Smith et al., 2018) as these algorithms tend to saturate in eutrophic condition.

Table 3
Threshold coefficients for QC test boundary lines. Figures in brackets indicate the minimum and maximum values for which each coefficient has been tested with the benefit function.

Algorithm	Boundary line	Threshold coefficients		
OC4	$L_{R12_{OC4}}(R53)$	$s = -0.12$ (−3–0)	$i = 0.99$ (0.79–1.14)	Linear regressions depending on R53
OC4	$L_{logR5_{OC4}}(R53)$	$s = 0.13$ (0–5)	$i = -2.26$ (−2.51 to −2.15)	
OC5	$L_{R12_{OC5}}(R53)$	$s = -0.62$ (−3–0)	$i = 0.85$ (0.79–1.14)	
OC5	$L_{logR5_{OC5}}(R53)$	$s = 0.73$ (0–5)	$i = -2.49$ (−2.51 to −2.15)	
OC5 RELAXED	$L_{logR5_{OC5}}(R53)$	$s = 0.66$ (0–5)	$i = -2.16$ (−2.51 to −2.15)	
NIR-RED	L_{Chl/NIR_RED}	8.1 (0.5–50)		Constant values
NIR-RED	L_{R6/NIR_RED}	0.0076 (0.0070–0.0085)		

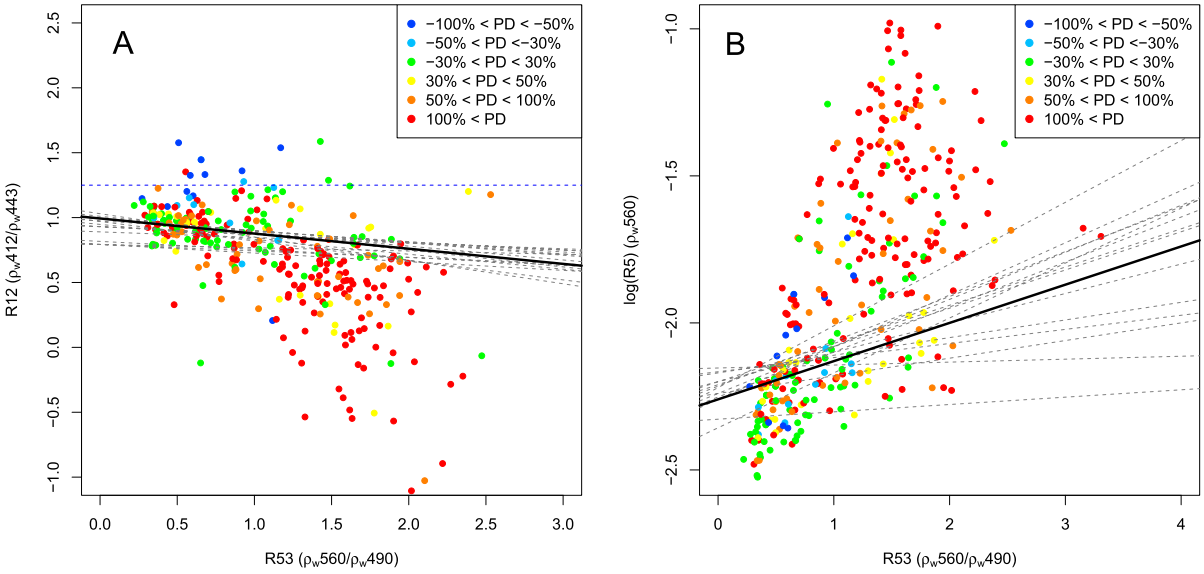

Fig. 4. R12 as a function of R53 (panel A) and $\log_{10}$(R5) as a function of R53 (panel B). The colour of dots refers to the percent difference (PD) between Chl-a from OC4 algorithm and in situ measurements. The grey lines show 20 examples of boundary lines (L_{R12_OC4} in panel A and L_{logR5_OC4} in panel B) generated in the subdivision-training-validation phase with 501 repetitions (see Section 2.3.3 for details). The thick black lines show final boundary lines (coefficients are given in Table 2). In panel A, the dashed blue line shows also the upper limit for R12 > 1.25 (suspect atmospheric correction). (For interpretation of the references to colour in this figure legend, the reader is referred to the web version of this article.)

Saturation is marked by constant CHL_OC4 values when in situ Chl-a increases (See Fig. 5aMatsushita et al., 2015). Such a saturation pattern is not observed in our dataset probably due to weak representation of eutrophic and hyper-eutrophic waters. However, to take into account all water conditions, a supplementary quality control test was introduced to verify that CHL_OC4 is lower than 10 mg.m^{-3}. The 10 mg m^{-3} was defined according to Smith et al. (2018). Finally, the QC procedure developed for the OC4 (and OC5) algorithm is summarized in the flowchart in Fig. 5.

3.1.2. QC test for OC5 algorithm

The OC5 quality control test was designed using the same approach as for OC4 and the final QC procedure is also displayed in the same flowchart as OC4 (Fig. 5). Fig. 6 shows that OC5 performs well for a wider range of R12 and R5 at a given R53 compared to OC4. The valid (green) points are more scattered and the boundary lines, L_{R12_OC5} and $L_{logR\_OC5,}$ are much less restrictive than for the OC4 algorithm, confirming that OC5 performs well for a larger range of CDOM and SPM values compared to OC4. For very low R12 and high log10(R5), OC5 tends to overestimate Chl-a motivating the need to also apply a QC test on OC5 Chl-a products.

To maximize the number of pixels processed especially during turbid conditions and because of the overall good performance of the OC5 algorithm on the present dataset, we propose an optional relaxed boundary line for the high SPM OC5 test (orange line in Fig. 6 panel B) computed by modifying the original BF (Eq. (6)) to a value of +5 for points with APD < 30%, +3 for points with APD between 30 and 50%, 0 to points with APD between 50 and 100% and − 2 to points with APD higher than 100%. The boundary line for the R12 test has not been modified as the standard version already accepts most of the dataset. The coefficients of the relaxed boundary line as well as the regular boundary lines are given in Table 3 and Section 3.2 presents the performance of OC5 when applying the relaxed QC.

3.1.3. QC test for NIR-RED algorithm

Fig. 7 shows the distribution of ρ_w620 as a function of CHL_OC4 with a colour code indicating the performance of the NIR-RED algorithm for each point. For low CHL_OC4 values (CHL_OC4 < 5 mg m^{-3}) and low ρ_w620 values ($\rho_w620 < 0.002$), NIR-RED fails for almost all points with a generally strong underestimation (dark blue points). Occasionally a strong overestimation (red points) is observed. It is clear that a certain threshold for CHL_OC4 and ρ_w620 is necessary to obtain accurate estimates of Chl-a by this algorithm. To determine this threshold BF was calculated for L_{Chl/NIR_RED} ranging between 0.5 and 50 by increments of 0.1 and for L_{R6/NIR_RED} ranging between 10^{-4} and 10^{-2} by increments of 10^{-4} and similarly to OC4 and OC5 protocol, values maximizing BF in each of the 501 simulations were retained. In 80% of the simulations performed, the thresholds limit $L_{CHL\_NIR\text{-}red}$ ranged between 7.6 mg m^{-3} and 10.2 mg m^{-3} and $L_{R6\_NIR\text{-}red}$ between 0.0072 and 0.0082. The final thresholds defined as the median of the 501 simulations are 8.1 mg m^{-3} and 0.0076 for $L_{CHL\_NIR\text{-}red}$ and $L_{R6\_NIR\text{-}red}$ respectively. Finally, an additional check was made to verify that the CHL_NIR-RED is at least higher

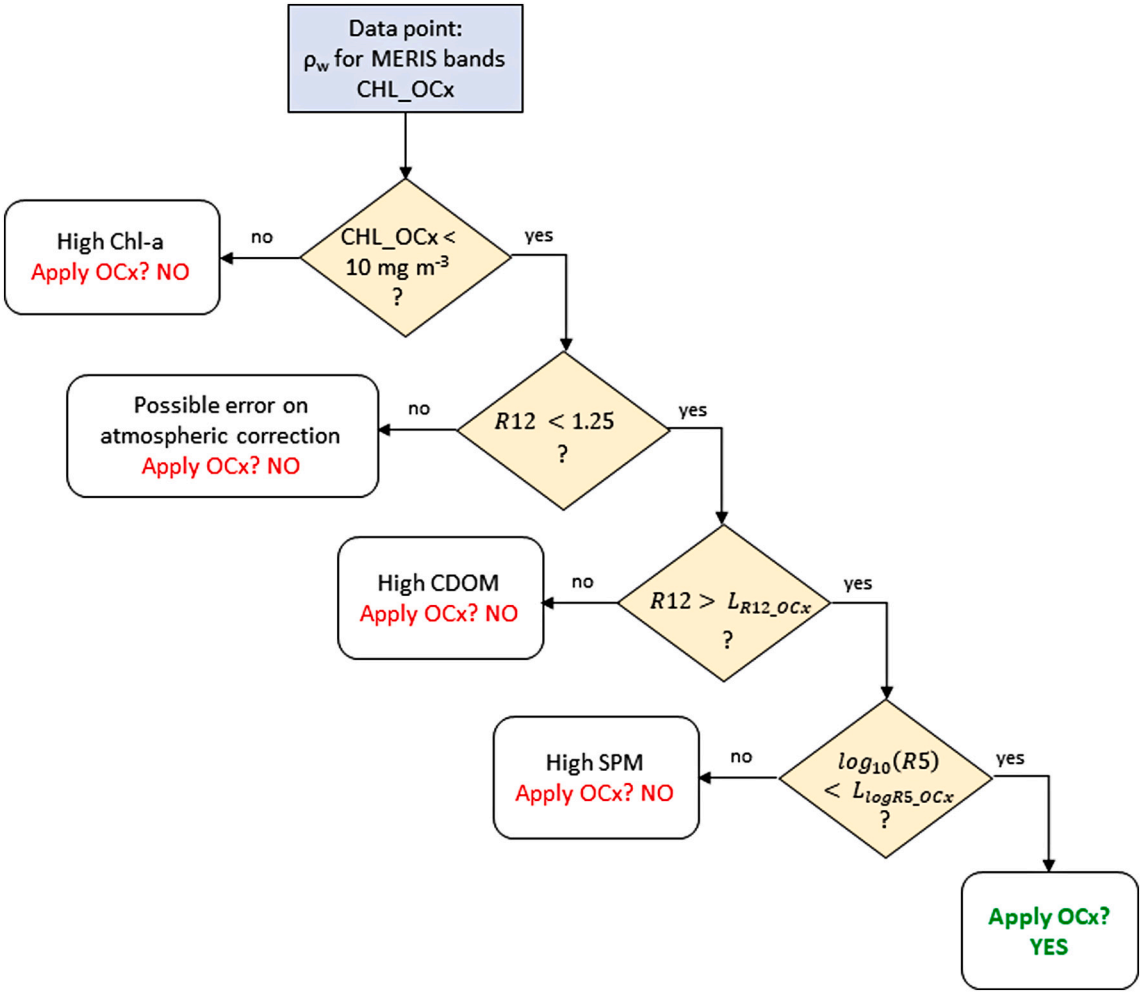

Fig. 5. Flow chart showing the different steps driving to the decision of application of the OC4 or OC5 algorithms. As QC steps are identical for OC4 and OC5 algorithms, only one chart is provided, the expression "OCx" in the chart can be replaced by either "OC4" or "OC5".

than 3 mg m^{-3}, considered here to be the detection limit for this algorithm (Gons et al., 2002). The different steps constituting the NIR-RED quality control are summarized in Fig. 8.

3.2. Performances of quality control tests

3.2.1. Performances of the OC4, OC5 and NIR-RED algorithms without quality control

The performances of the OC4, OC5 and NIR-RED algorithms were initially tested using the whole CCRR-MERMAID matchup dataset without application of quality controls (Fig. 2, Table 4). The results show that without QC the OC5 algorithm performs best with a median absolute percent difference of 39% and a slight overestimation (median ratio = 1.17). Most of the points were situated close to the 1:1 line and the RMSD was 2.36 mg m^{-3}. The OC4 algorithm clearly tends to overestimate Chl-a concentration as most of the points were above the 1:1 line and the median ratio is 1.84, resulting in a MAPD of 84.5%, which is significantly greater than in case 1 waters (i.e. 35%, Bailey and Werdell, 2006), with a rather scattered distribution (RMSD = 5.53 mg m^{-3}). These results confirmed the previously observed tendency of the OC4 algorithm to overestimate Chl-a concentration in coastal waters (Tilstone et al., 2017) and as expected, the OC5 algorithm tends to correct this overestimation. The performance of the NIR-RED algorithm confirms expected patterns (Ruddick et al., 2001; Gons et al., 2008; Smith et al., 2018) with strongly scattered and erroneous Chl-a estimates for low to moderate Chl-a values (Chl-a < 10 mg m^{-3}). In fact, only high in situ Chl-a values have satellite estimates near the 1:1 line. As it is well known that Chl-a algorithms based on NIR-RED band ratio are only designed for eutrophic waters, the lower limit (Chl-a = 3 mg m^{-3}) that is recommended to consider when using NIR-RED algorithm (Gons et al., 2002) is drawn on Fig. 2 panels C and F (grey dotted lines) and used for calculation of validation statistics (Table 4). Although this limit allows to eliminate all negative and low estimates, it also shows that without a priori information on a study area the elimination only of CHL_NIR less than 3 mg m^{-3} can still led to very high overestimation errors (Fig. 2C; Table 4).

The moderate to bad performances of the OC5, OC4 and NIR-RED algorithms on the whole coastal dataset demonstrate the importance of defining quality control tests for each of these algorithms and for preventing use of their outputs when not appropriate.

3.2.2. Performances of the OC4, OC5 and NIR-RED algorithms after application of quality control

Fig. 9 shows the distribution of each performance metric when applied to the validation dataset (50% of the whole CCRR-MERMAID dataset) before (blue boxplots) and after applying the QC (yellow boxplots) obtained for the 501 simulations. For the OC4 and NIR-RED algorithms, the boxplot comparison shows a clear improvement of all metrics after QC. Results for the OC5 algorithm also show a positive evolution as application of QC reduces the positive bias (MR is reduced), as well as the uncertainty (reduced RMSD) and the median percent difference. Only r^2, the coefficient of determination of the linear

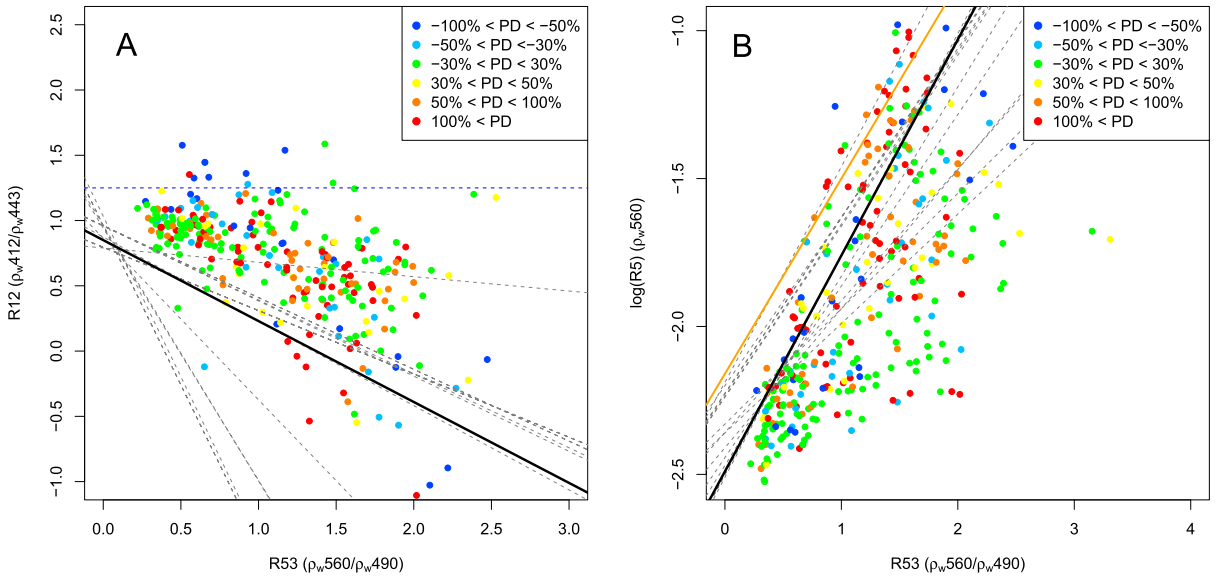

Fig. 6. R12 as a function of R53 (panel A) and log(R5) as a function of R53 (panel B). Colour of dots refers to the percent difference (PD) between Chl-a from OC5 algorithm and in situ measurements. Grey lines show 20 examples of limit curves (L_{R12_OC5} panel A and L_{logR5_OC5} panel B) produced in the subdivision-training-validation phase out of 501 repetitions (see Section 2.3.3 for details). The thick black lines show final boundary lines (coefficients are given in Table 2). In panel A, the dashed blue line shows also the upper limit for R12 > 1.25 (suspect atmospheric correction). The orange dotted line in panel B represent the boundary line in case of use of the relaxed version of the OC5 algorithm. This additional boundary line has been calculated by modifying the benefit function (see Section 3.1.2 for details). (For interpretation of the references to colour in this figure legend, the reader is referred to the web version of this article.)

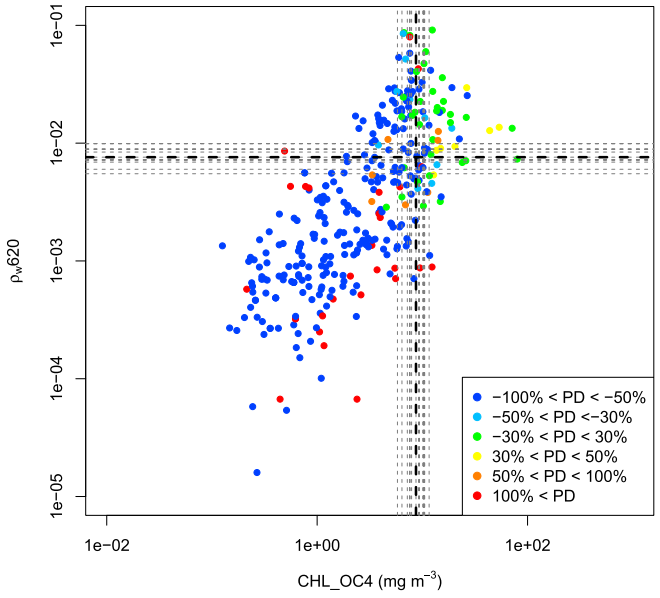

Fig. 7. ρ_w620 as a function of CHL_OC4. Colour of dots refers to the percent difference (PD) between Chl-a from NIR-RED algorithm and in situ measurements. Grey lines show 20 examples of boundary lines for CHL_OC4 (vertical lines) and ρ_w620 (horizontal lines) computed during the division-training-validation phase. Thick black dashed lines show the final boundary lines.

regression between in situ and satellite measurements, as well as the slope and the intercept of the linear regression are not significantly improved when computed from QC positive data points only. This effect can be explained by the fact that the Chl-a range is slightly reduced (all points with CHL_OC5 > 10 mg m^{-3} are eliminated). As expected OC4 and NIR-RED quality controls are the most drastic as they retained only 20% and 13% of dataset respectively. This result is easily explained by the low occurrences of case 1 and hyper-eutrophic conditions in coastal waters in general and hence in the CCRR-MERMAID dataset. On the contrary, the OC5 algorithm is better adapted to moderately turbid waters characterizing most of the coastal waters and applies after QC to 64% of the dataset. In addition, 50 additional points (13% of the dataset) can be added if relaxed OC5 QC is applied. For these extra points, Chl-a derived from OC5 is generally overestimated (MR = 1.5) and MAPD increases to 57% which might remain acceptable for certain applications. Table 4 indicates performance of the final QC when applied to the full CCRR-MERMAID dataset in comparison to the absence of QC and Fig. 10 (panels A, B and C) show for each algorithm which datapoints have been pass QC tests (red dots). These graphs show that after QC a majority of dots are in the −50%/+50% percent difference which is positive. However, some "good datapoints" don't pass QC, suggesting the limits of the present QC tests. This could be explained by natural variability, uncertainty of in situ measurements or error in the retrieval of water leaving reflectance. Looking at statistical metrics (Table 4), the overall positive impact of QC tests observed with the training/validation exercise is confirmed (Fig. 9) and metrics show almost unbiased Chl-a estimations when QC is applied (MR varies between 0.9 and 1.17), MAPD is reduced to the 30–34% range and RMSD which can be considered as a measure of uncertainty is about 1 mg m^{-3} for OC4 and OC5 algorithms and 5 mg.m^{-3} for the NIR-RED algorithm which is adapted to the high Chl-a values processed by NIR-RED algorithm.

Fig. 11 shows how after QC tests the OC4, OC5 and NIR-RED algorithms are geographically distributed in the north hemisphere. Results show that no algorithm is restricted to a specific region. OC5 the most widespread algorithm is applied along California coast, in the Gulf of Mexico, in Mediterranean and Black Sea, along Atlantic European coast from Spain to Denmark as well as the North Sea and Baltic sea. As expected, OC4 is mostly used in the clear oligotrophic waters of the Mediterranean Sea, Californian coast and South Portugal coast and NIR-RED algorithm mostly applied in very coastal regions of the North Sea, French Atlantic coast, North East American coast. The method of Chl-a measurement (i.e. HPLC, fluorometry or spectrophotometry) seems to be independent of the selected algorithm. These results tend to confirm that the developed QC tests are based on optical water types rather than strong regional specificities or inconsistencies between sub-datasets that made the CCRR-MERMAID database.

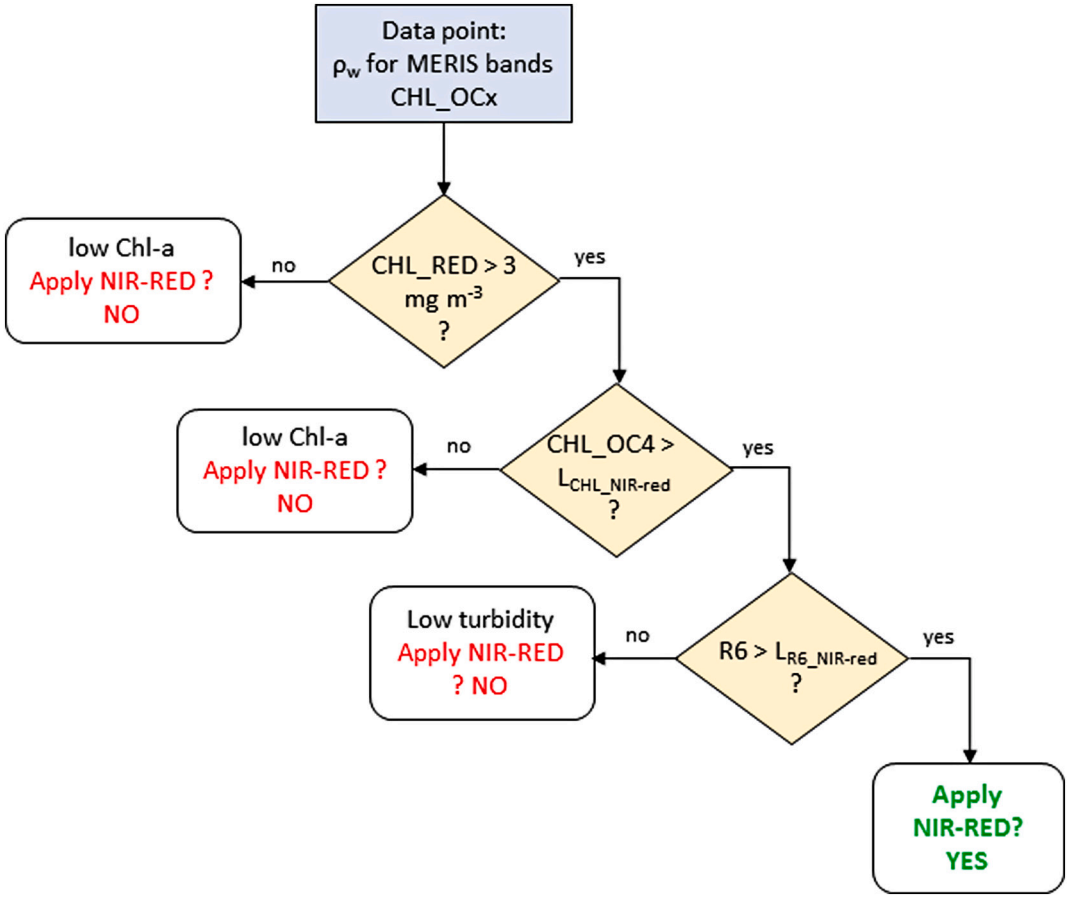

Fig. 8. Flow chart showing the different steps driving to a decision of application of the NIR-RED algorithm.

Table 4
Performances of the OC4, OC5 and NIR-RED algorithms when they are tested against the whole dataset before and after applying QC tests (referred with the "QC" mention). "merged" and "merged / OC5 extended" refers to the multi-algorithm merged products described in Section 3.2.3. "N" indicates the number of matchups. This number is reduced when QC tests are applied and for NIR-RED algorithm where only matchups with CHL_RED higher than 3 mg / m^{-3} are selected.

	N	MR	MAPD	slope	intercept	RMSD	r^2	p_{value}
OC4	348	1.84	84.5%	1.46	1.47	5.53	0.53	>2.2 10^{-16}
OC5	348	1.17	39.1%	0.85	0.59	2.36	0.69	>2.2 10^{-16}
NIR-RED[1]	77	1.43	53%	−2.7	56.6	95.4	0.04	0.094
OC4 QC	69	1.17	34.7%	1.21	0.10	0.85	0.78	>2.2 10^{-16}
OC5 QC	222	1.07	30.5%	0.56	1.03	1.59	0.55	>2.2 10^{-16}
NIR-RED QC	46	0.92	30.5%	1.06	−0.94	4.90	0.71	2.9 10^{-8}
Merged algorithm	244	1.08	30.4%	0.96	0.25	2.37	0.77	>2.2 10^{-16}
Merged / OC5 relaxed	292	1.16	33.8%	0.95	0.34	2.24	0.76	>2.2 10^{-16}

[1] Only datapoints with a NIR-RED Chl-a estimation higher than 3 mg m^{-3} were considered following the recommendation of Gons et al. (2002).

3.2.3. *Merged algorithm*

After application of QC, 70% of the dataset (242 data points) can be processed by at least one of the OC4, OC5 and NIR-RED algorithms and this number increases up to 83% (290 data points) if the relaxed version of the OC5 QC is applied. Although each algorithm performs better in specific water types, some data points can pass two different algorithms QC. In fact, all points (69 points in the CCRR-MERMAID dataset) which pass QC for OC4 also pass QC for OC5. Additionally, 14 points passed the QC for both OC5 and NIR-RED and no point passed the QC for all three algorithms (i.e. OC4, OC5 and NIR-RED). To create a merged product, these specific points were naïvely treated by averaging over the two valid algorithms. Although many much more complex methods have been used to merge Chl-a algorithms (Gons et al., 2008; Hieronymi et al., 2017; Smith et al., 2018), we chose to use simple averages because (1) the main scope of this paper is to provide independent QC tests for a series of Chl-a algorithms and (2) our present dataset was insufficient for testing more sophisticated merging methods. This task of algorithm merging is further discussed in Section 4.2. The performance of the final merged algorithm after QC is presented on Table 4 (lines 7 and 8) and Fig. 10 (panel D). The standard merged algorithm has a median absolute percent difference of 30.4% and the points are well aligned along the 1:1 line (see Fig. 10 and Table 3; r^2 of the linear regression = 77%). 68% of the data points are within the plus or minus 50% APD range. The majority of points out of this range present an overestimation of the in situ Chl-a measurements. When OC5 standard QC is replaced by the relaxed version, performance is only slightly reduced with a median absolute percent difference of 33.8% and a slight overestimation (MR = 1.16). Finally, whatever the version of the merged algorithm, the performance is comparable to that obtained in case 1 waters (O'Reilly and Werdell, 2019).

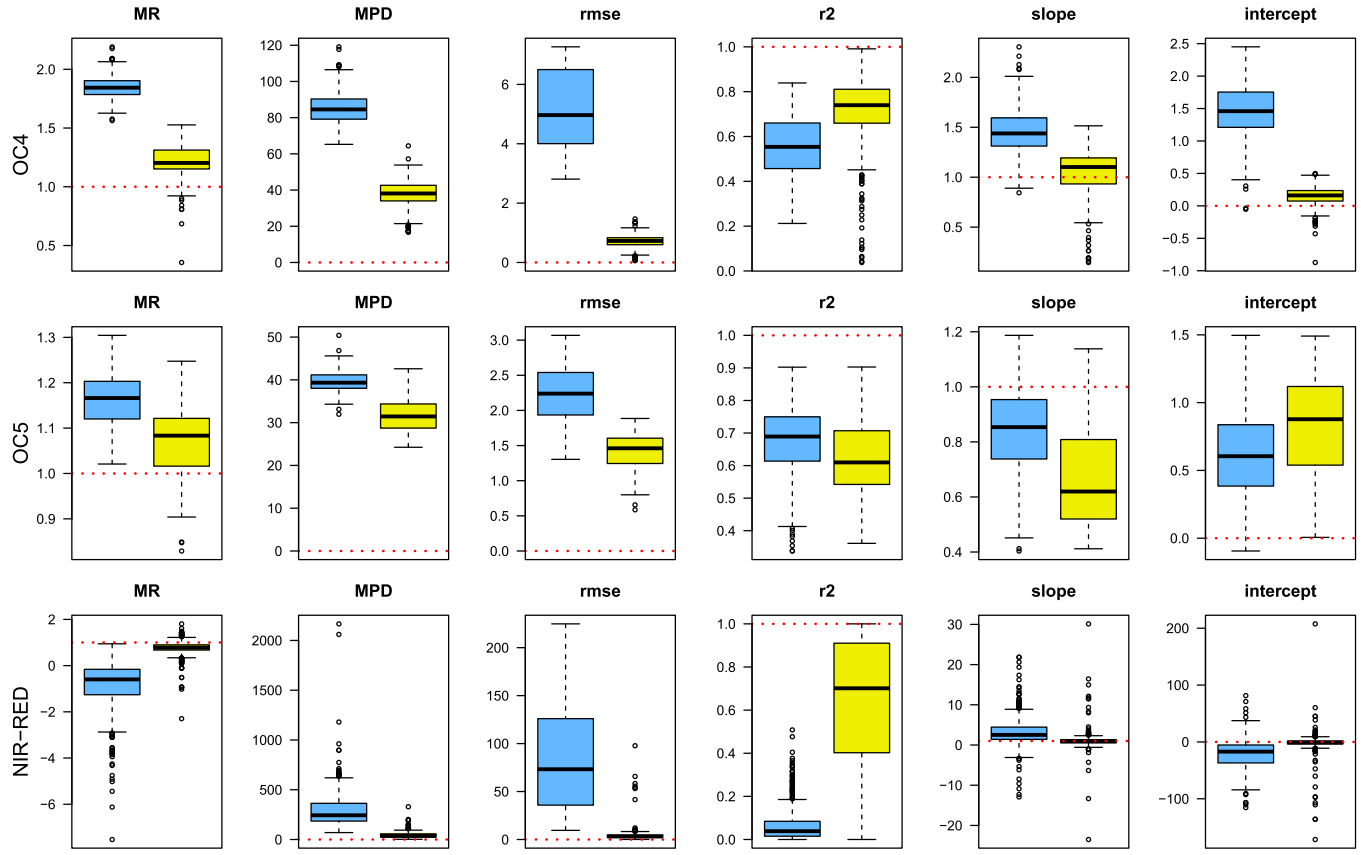

Fig. 9. Box-plots comparing the performances of the OC4 (top panels), OC5 (middle panels) and NIR-RED (bottom panels) algorithms on the initial validation dataset (blue box-plots, 50% of the whole CCRR-MERMAID dataset randomly defined in the division-training-validation phase) to the subset of points having passed the QC (yellow box-plots). In the case of the NIR-RED algorithm before QC (blue boxplots), statistics were calculated for datapoints with a NIR-RED Chl-a value higher than 3 mg m^{-3} following Gons et al. (2002). By this way, negative values are removed. The red dotted lines represent for each metric its ideal values in case of a perfect algorithm. Note that the y-axis scales differ for some metrics between algorithms. (For interpretation of the references to colour in this figure legend, the reader is referred to the web version of this article.)

3.3. Application to satellite data

3.3.1. Application to MERIS data

Four almost cloud-free images of the North-Western European waters were selected from the MERIS MEGS8 RR Level 2 archive to illustrate application of the QC tests. The QC test for each Chl-a algorithm and the proposed algorithm merging approach were applied to each image in order to generate final Chl-a maps (Figs. 12 and 13). The results show that the OC5 algorithm is used in most regions and for most times of the year with a few exceptions. Due to high turbidity, the image of 2006-03-06 shows that Chl-a concentration can be processed only if the relaxed condition for the OC5 algorithm is applied. In addition, some areas flagged as "high SPM" with the OC5 algorithm cannot be processed by any of the three Chl-a algorithms presented here. These areas generally correspond to very turbid zones visible on the RGB true colour image (see Fig. S1 / Supplementary material). In the image of 2004-05-24, a large offshore area along the French Atlantic coast (46°N, 4°W) was also flagged as "No algorithm" surrounding by "OC5 relaxed". This spot which occurs during the spring bloom season was identified as a coccolithophorid bloom from the RGB image (see Fig. S1). Coccolithophorids have calcified scales (coccoliths) causing very high scattering, affecting standard Chl-a algorithms and explaining the flag "high SPM" returned by the OC5 QC test. OC4 was mostly applied in the images of 2007-08-11 and 2005-09-19 offshore of the French Atlantic coast (around 46°N/5°W). In this season, the main rivers have low discharge and offshore Atlantic waters are expected to be close to case 1 waters. The NIR-RED algorithm was applied to some nearshore areas and river estuaries and plumes. The Thames Estuary (52°N/1°E), the Humber Estuary (53.5°N/0°E) and the Severn Estuary (52°N/3°W) show large NIR-RED algorithm areas in the 2006-03-06 image. NIR-RED algorithm also applies is Belgian coastal waters and the Dutch Wadden Sea (52°N/3°E and 53°N/5°E respectively) in images 2004-05-23, 2007-08-11 and 2005-09-19. For the selected images Fig. 13 shows that Chl-a ranges between 0.5 and more than 8 mg m^{-3} with highest values along the coast between 51°N and 54°N. In the English Channel (50°N/3°W) and the central North Sea (52°N/3°E), Chl-a is highest in the 2004-05-23 and 2007-08-11 images with values reaching 3 mg m^{-3} in the English Channel and more than 7 mg m^{-3} in the North Sea.

3.3.2. Application to OLCI data

A first application of the algorithm QC and merging approach applied to OLCI-A data is presented in Fig. 13 for an image acquired on 2017-06-18. L1 reduced resolution data were processed to level 2 with the POLYMER atmospheric correction processor (Steinmetz et al., 2011). This atmospheric correction algorithm is designed for coastal waters and has shown good results for OLCI data when compared to AERONET-OC data (Zibordi et al., 2009) located in the North Sea (Cardoso Dos Santos et al., 2019). Although a future calibration of OLCI CHL_OC5 is required, OC5 look-up tables published for MERIS were applied to OLCI data, which has very similar spectral bands. The spectral similarity between MERIS and OLCI sensors was tested on a large number of hyperspectral in situ reflectance spectra measured in coastal waters and contrary to observations reported by Wang et al. (2020) when comparing OLCI and VIIRS spectral band, no band shift was

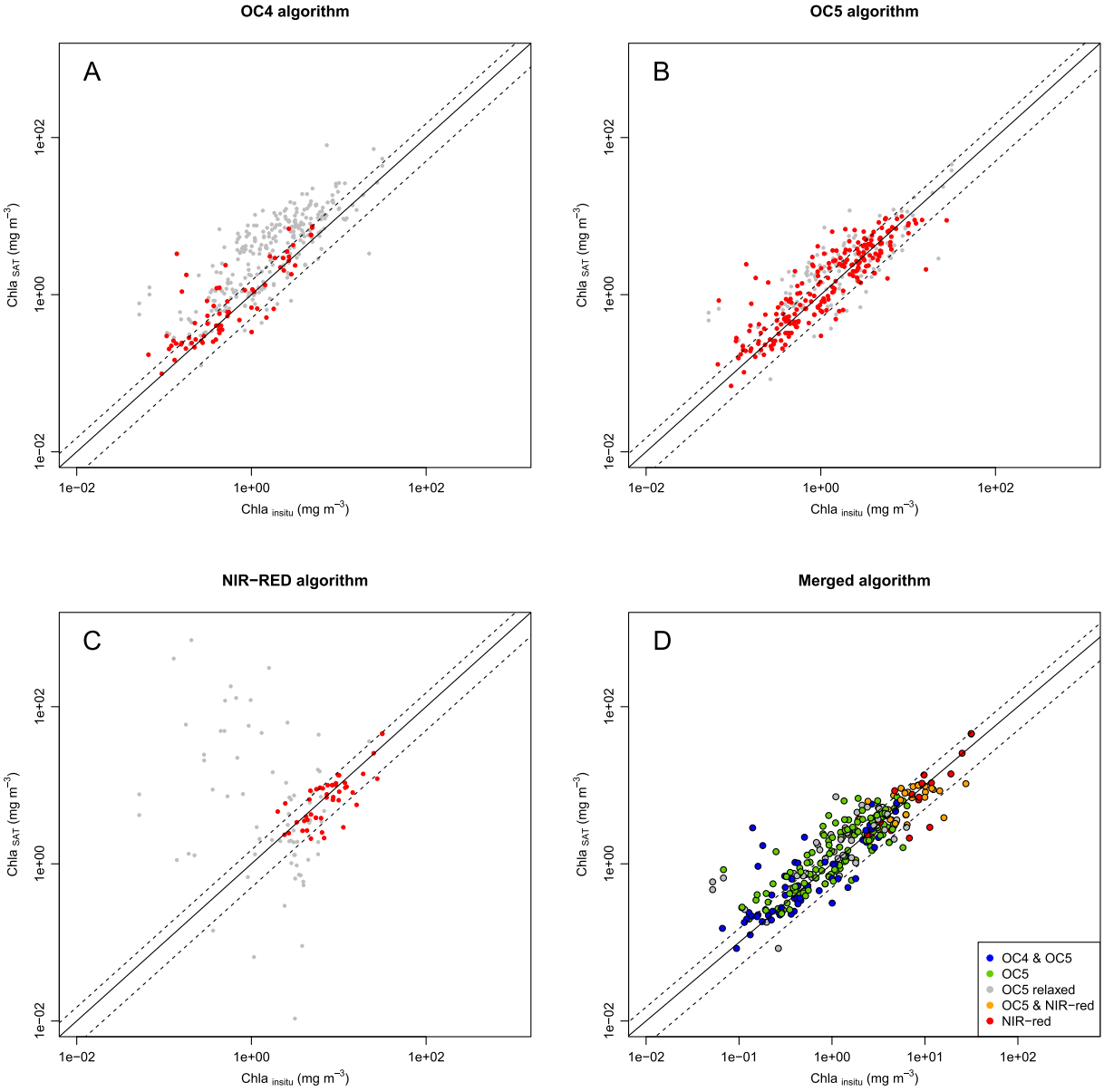

Fig. 10. In situ Chl-a observations as a function of satellite Chl-a estimations. In panels A to C, red dots represent datapoints which pass the final OC4, OC5 and NIR_RED QC respectively, whereas greys points didn't pass QC. Panel D shows In situ Chl-a observations as a function of satellite Chl-a estimations after application of QC tests and merging methodology presented in this paper. Colour code indicates for each point which Chl-a algorithm has been selected. 292 points (83% of the full MERMAID-CCRR dataset) are represented here. The validation metrics are provided in Table 4 lines 7 and 8 for standard merged algorithm and extending version respectively. In each panel, dotted lines represent the ±50% error interval. (For interpretation of the references to colour in this figure legend, the reader is referred to the web version of this article.)

observed between MERIS and OLCI (Table S1, supplementary material). Fig. 14 shows a large region application of the OC5 algorithm with some areas offshore of the French and UK coasts where the OC4 algorithm is also valid. Along the coast, the OC5 algorithm is accepted in its relaxed version due to higher turbidity. In some offshore areas of the northern North Sea (58°N/2°W) and west of England (51°N/5.5°W) only the relaxed version of OC5 algorithm is accepted. RGB image (Fig. S2 / supplementary material) indicates that these areas correspond to Coccolithophorid blooms. Finally, the NIR-RED algorithm is selected in the Wadden Sea north of the Netherlands (53°N/5°E). The Chl-a map shows values ranging between 0.15 and 8 mg m^{-3}, with, similarly to the MERIS images, highest Chl-a value along the coast close to estuaries and higher Chl-a values in the southern North Sea (52°N/3°E) than in the English Chanel (49°N/5°W). The results presented here need to be validated against in situ measurements, which are not available yet, but as a first observation they are consistent with MERIS results and suggest that the present methodology should be easily applicable to OLCI and hence ensure reliable Chl-a data over the next decades.

4. Discussion

4.1. Discussion on methodology

We propose QC tests based on the relative percent difference between in situ and satellite estimates to prevent use of three different Chl-a algorithms outside their conditions of validity and to prevent the production of erroneous remote sensing Chl-a products in coastal waters. The QC tests have been designed here on the basis of MERIS/in situ matchups for coastal waters. In contrast to the simulated datasets generated from radiative transfer models (Doerffer and Schiller, 2007;

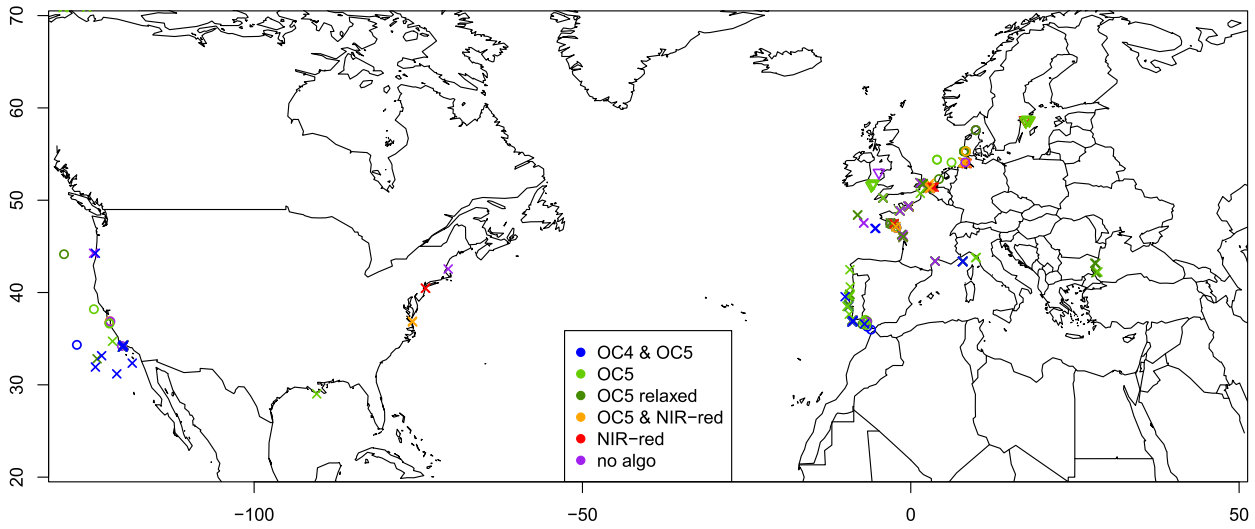

Fig. 11. Geographic distribution of CCRR-MERMAID data in the north hemisphere (north hemisphere contains a large majority of the CCRR-MERMAID database, see Fig. 1). The Colour code indicates for each data point which algorithm have been selected by QC tests. Symbol shape indicates the method of measurement of in situ Chl-a (cross: HPLC, circle: fluorometry, triangle: spectrophotometry).

Nechad et al., 2015; Hieronymi et al., 2017) which are often used for algorithm testing, the CCRR-MERMAID dataset used here is based on MERIS water reflectance. This choice of dataset solves any application transfer issue which may arise from algorithms developed based on synthetic datasets because of possible bias in the representation of optical processes in the radiative transfer models. Nonetheless, as is generally the case for in situ/satellite matchup datasets, the CCRR-MERMAID dataset presents geographic limitation. Indeed, the CCRR/MERMAID dataset is dominated by the North Sea and European Atlantic coast with respectively 38% and 24% of data points whereas the other regions are also represented (Californian coast, 22% of data points; Mediterranean Sea, 12.5% of data points and North America east coast, 2%). However, the over-representation of North European waters in the dataset shouldn't be an issue for global application, as North European waters cover a large range of optical water conditions (Hieronymi et al., 2017Fig. 6; Mélin and Vantrepotte, 2015) with the presence of very turbid, absorbing or eutrophic waters. Regarding the OC5 algorithm, although it has been parameterized from a regional dataset (Gohin et al., 2002) located in the North European waters and there might be concerns about extrapolation to other regions, OC5 has also been successfully validated and/or applied in many other regions such as the Bay of Bengal and Arabian Sea (Tilstone et al., 2011); the Southern Bay of Biscay (Novoa et al., 2012; the Mediterranean Sea (Druon et al., 2004; Fraysse et al., 2014) or the Gulf of Gabes (Katlane et al., 2012). OC5 only failed to retrieve Chl-a concentration in the extremely turbid waters of the Rio de la Plata in Argentina (Camiolo et al., 2016) but this result supports the QC tests presented in this paper which indicate that for extremely turbid conditions the OC5 algorithm cannot be used.

Indeed, while the OC5 algorithm is by far the best performing algorithm in most coastal waters, there is value in using additional algorithms because in certain specific conditions OC5 would result in erroneous estimates with a significant overestimation of Chl-a (extremely turbid waters, Camiolo et al., 2016) or a significant underestimation of Chl-a (hyper-eutrophic water, Tilstone et al., 2017). For certain applications like eutrophication monitoring such errors could have critical consequences as it is very important to assess hyper-eutrophic regions well even if they only represent a small number of pixels. Then, whatever the algorithm, it is important to determine a domain of validity and to propose alternative algorithms when possible.

The huge number of Chl-a algorithms developed for case 2 waters (Odermatt et al., 2012; Neil et al., 2019), were dramatically reduced for study here three algorithms based on the following criteria. First, as explained in Section 2.3.1., an a priori knowledge about the conditions of application and limits of the algorithm was needed. Following this criterion, algorithms such as neural networks (i.e. Doerffer and Schiller, 2007; Hieronymi et al., 2017) were screened out. Next, only algorithms with a potential for global application were retained and finally, to avoid too much complexity, only one algorithm was selected in a same group of algorithms (i.e. algorithms based on the same theory and applicable to the same type of waters such as blue-green band ratio algorithms or NIR-red band ratio algorithms). However, results for additional algorithms in the OC4 and NIR-RED categories are discussed hereafter.

OC4 has been selected for its very strong popularity (O'Reilly et al., 1998) and accessibility compared to OC5 which is based on LUTs and might be less easy to compute for some users although OC5-Chl-a products are distributed by the Copernicus Marine Environment Monitoring Service (CMEMS, http://marine.copernicus.eu/). Recently, a new algorithm called "OC6" has been published by O'Reilly and Werdell (2019). This algorithm, dedicated to clear waters, is derived from OC4 but uses two additional bands: 412 nm and 665 nm which could give better results in coastal waters. However, a first test has shown that after applying a dedicated QC similar to the QC developed for OC4 and OC5, OC6 algorithm performance was not improved (see Fig. S3/supplementary materials). Based on these results we decided not to further analyse OC6 in this study, although it may be relevant to revisit OC6 at a later stage. The NIR-RED Gons (1999) algorithm has been selected for its complementarity with OC5 and OC4 in hyper-eutrophic waters (Gons et al., 2008; Smith et al., 2018) and its semi-analytical basis. However, there is a large range of NIR-RED algorithms (Dall'Olmo et al., 2005; Gitelson et al., 2007; Moses et al., 2009; Le et al., 2009; Gilerson et al. 92010; Gurlin et al., 2011), that are all adapted to turbid eutrophic waters. To complete the present analysis, 2-bands and 3-bands semi-analytical algorithms presented by Gilerson et al. (2010) were also tested. Whereas the 2-band Gilerson et al. (2010) algorithm is very similar to the Gons (1999) algorithm as they both use the reflectance band ratio 709 nm over 665 nm, the 3-band Gilerson et al. (2010) algorithm is based on a different structure which was designed to perform better in the case of non negligible absorption due to non algal particles and CDOM (Dall'Olmo et al., 2005). Contrary to Gons (1999) algorithm, Gilerson et al. (2010) algorithms account for variations with Chl-a of the phytoplankton specific Chl-a absorption coefficient (Bricaud et al., 1998). The same procedure as the one applied to NIR-RED algorithm, was applied to the Gilerson et al. (2010) 2-band and 3-band algorithms. Final boundary lines and performances statistics obtained after

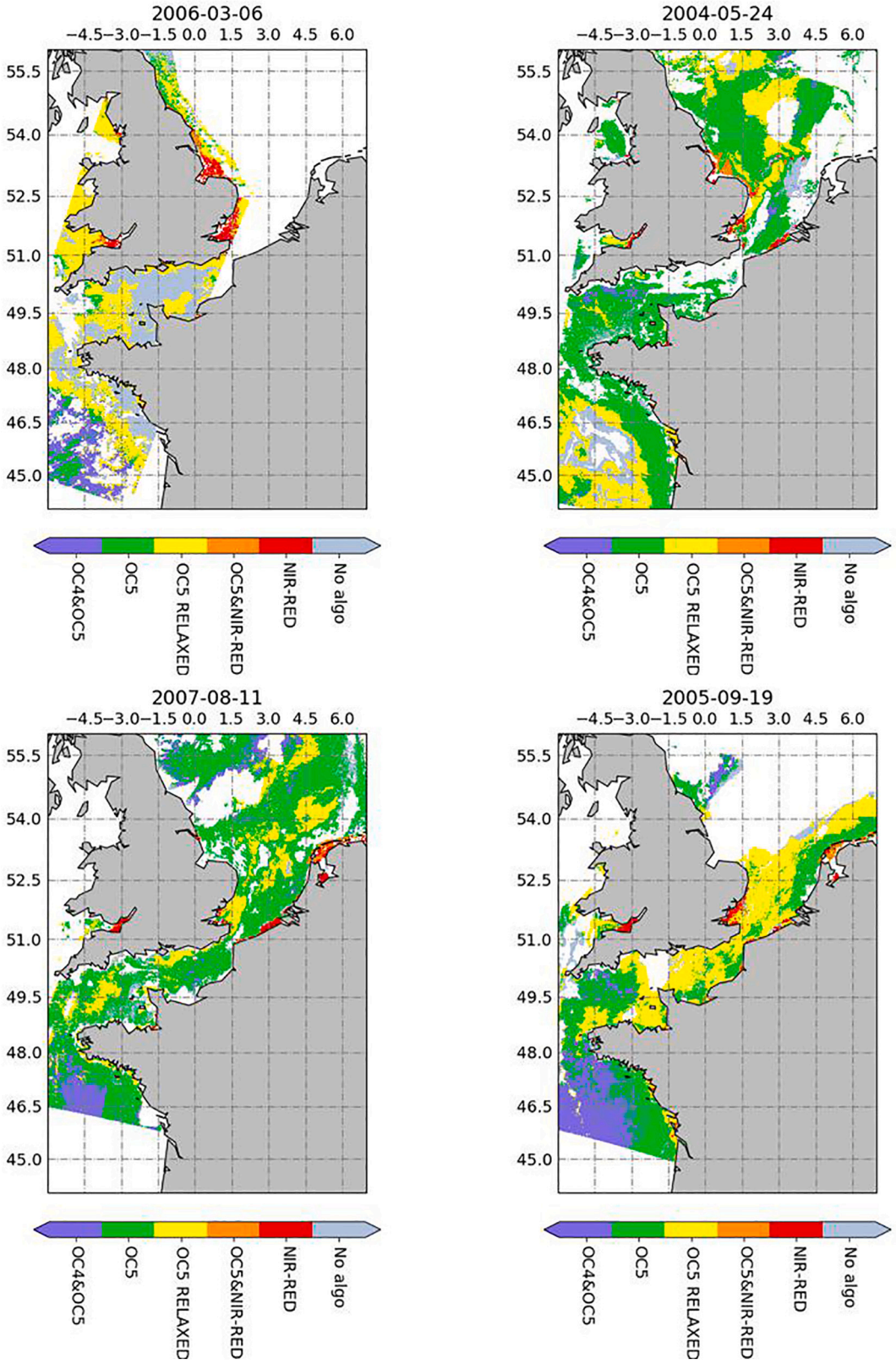

Fig. 12. Results for the Chl-a switching algorithm methodology developed in this paper and applied to 4 MERIS images processed from ODESA (http://www.odesa-info.eu/info/) with MEGS8.1 version. Land is shown in grey. No reflectance data are available for the white areas (clouds, sunglint, atmospheric correction failure, outside swath, etc.). Colour indicates which algorithm(s) pass QC. The corresponding RGB images are available in supplementary materials (Fig. S1).

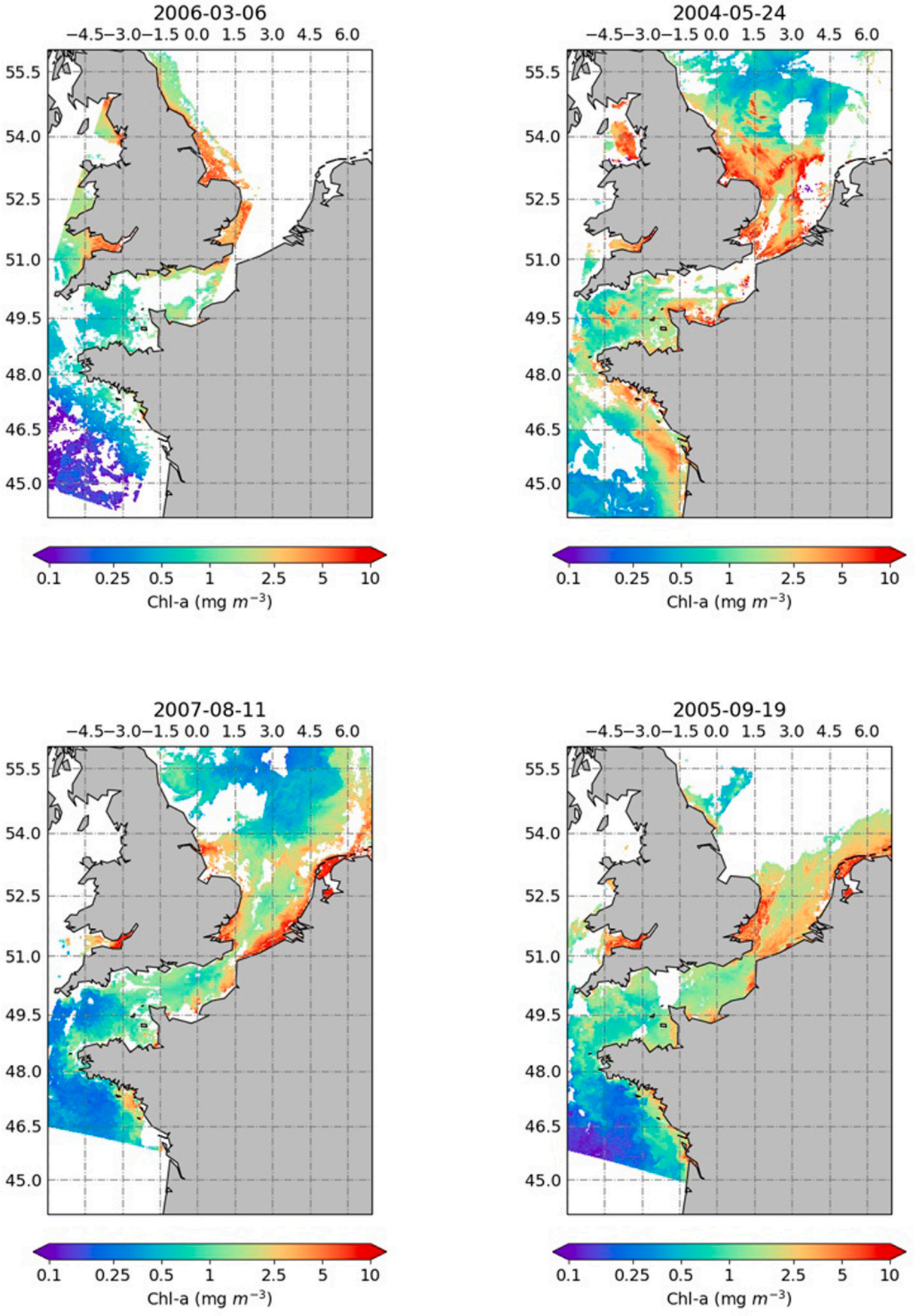

Fig. 13. Merged Chl-a maps derived using the switching algorithm approach and applied to the same images as shown in Fig. 12. White areas are where input reflectance data was missing or no Chl-a algorithm passed QC. Corresponding RGB image is available in supplementary materials (Fig. S1).

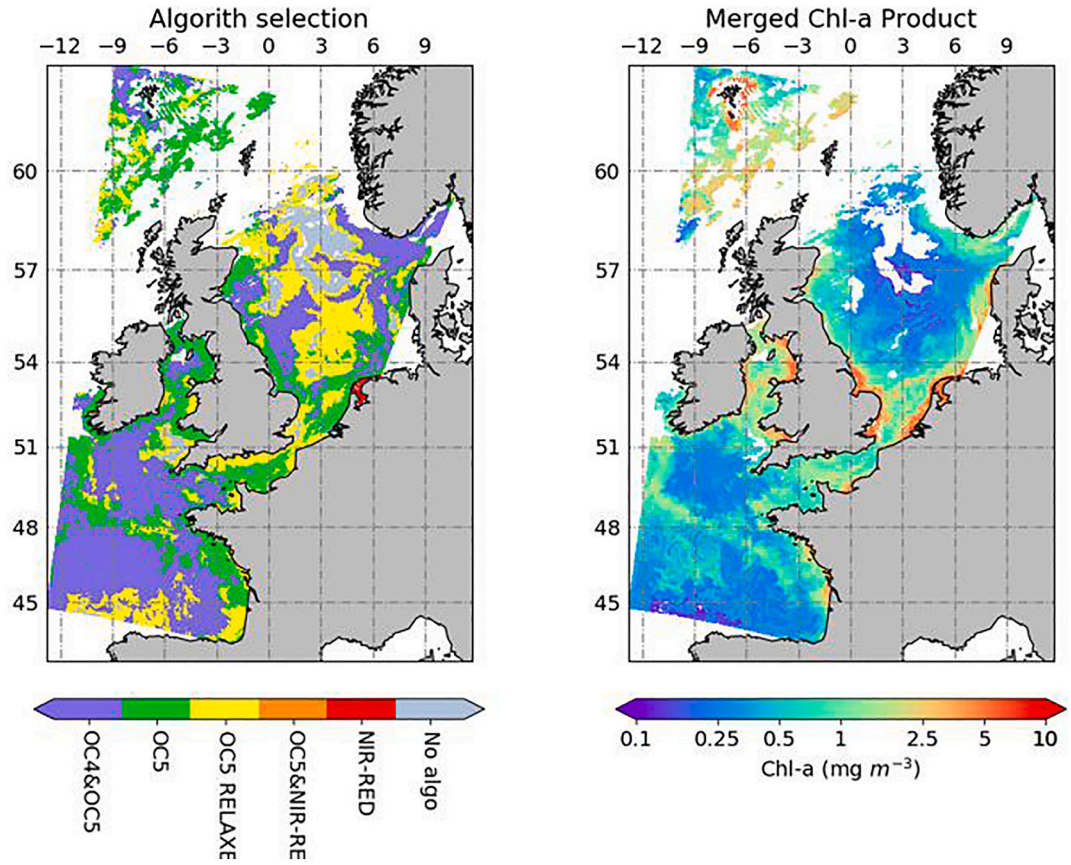

Fig. 14. Application of the Chl-a algorithm methodology developed in this paper to OLCI reduced resolution image data from 2017 to 06-18. The left panel shows algorithm selection and the right panel shows the resulting merged Chl-a map. The OLCI image has been processed from level 1 with the POLYMER atmospheric correction (Steinmetz et al., 2011). Corresponding RGB image is available in supplementary materials (Fig. S2).

application of dedicated QC are presented in Table 5. Results show that the 2-band Gilerson et al. (2010) algorithm is the one which allows to accept the most datapoints (54) with the less restrictive boundary lines although the performances are slightly degraded compared to Gons et al. (2005) and Gilerson et al., 2010 3-band algorithms. Gilerson et al. (2010) 2-band algorithm and NIR-RED algorithm (Gons et al., 2005) which are both based on the same reflectance ratio show very similar results and an end-user according to its preference could use either one. Gilerson et al. (2010) 3-bands algorithm shows very restrictive QC which reduces the interest of this algorithm in this context (i.e. coastal waters and application of QC).

Finally, it is noted that the present QC are designed for coastal waters and are not optimal for ultra-oligotrophic case 1 waters (i.e. Chl-a $<$ 0.25 mg m^{-3}). For case 1 waters we would recommend the users to simply use the OC4 algorithm, or to apply the colour index (CI) approach (Hu et al., 2012) as it has already been implemented in several satellite Chl-a products (i.e. CMEMS products: Volpe et al., 2019, Globcolour products: Garnesson et al., 2019; NASA products: https://oceancolor.gsfc.nasa.gov/atbd/chlor_a/).

4.2. Quality control tests versus merged algorithms

In this study, we present an approach based on quality control tests for OC4, OC5 and NIR-RED algorithms on a pixel-by-pixel basis. Indeed, contrary to many multi-algorithm approaches previously developed (Gons et al., 2008; Kahru and Mitchell, 2010; Hieronymi et al., 2017; Smith et al., 2018), our first objective was not to create a merged algorithm but to provide to future users a simple way to ensure that Chl-a values calculated by OC4, OC5 and NIR-RED algorithms are reliable. Hence, the QC tests proposed here are independent of each other and can be used on their own. However, as OC4, OC5 and the NIR-RED algorithms perform better in different water types, it makes sense to combine them to process satellite images. A simple combination method based on averages has been presented in the Section 3.2.2 and applied to MERIS and OLCI images (Section 3.3). Although results showed coherent maps, the QC may produce discontinuities in Chl-a concentration when switching between two algorithms and creates white areas where no algorithm applies. To fill white areas, it is possible to relax the benefit function as it was done for OC5 while increasing uncertainty or to develop specific algorithms for optical waters that do not pass QC

Table 5
Performances and threshold coefficients for QC tests of three chl-a algorithms based on red-edge reflectance. The Gons et al. (2005) algorithm is the NIR-RED algorithm studied in this paper (Section 3), performance statistics and QC limits have been copied from Tables 3 and 4 to facilitate comparison.

Algorithm	Threshold coeffcients		Validation statistics after QC						
Reference	L_{Chl/NIR_RED}	L_{R6/NIR_RED}	N	MR	MPD	slope	int.	RMSD	r^2
Gons et al., 2005	8.1 mg m^{-3}	0.0076	46	0.92	30.5%	1.06	−0.94	4.90	0.71
Gilerson et al., 2010 (Eq. 17.2, 2-band)	6.9 mg m^{-3}	0.0065	54	1.23	33.9%	1.26	0.23	5.35	0.73
Gilerson et al., 2010 (Eq. 19.2, 3-band)	14.6 mg m^{-3}	0.0086	14	1.10	29.9%	1.16	−1.37	7.3	0.73

conditions for OC4, OC5 and NIR-RED. However, it is important to recognise that the ocean colour satellite measurement technique simply cannot be used for Chl-a when phytoplankton does not significantly affect the water reflectance. Then, in some cases white areas are unavoidable with current satellite sensor technology.

Transition between algorithms have been addressed in previous studies with the utilization of weighting approaches to merge different Chl-a algorithms (Gons et al., 2008; Hieronymi et al., 2017; Smith et al., 2018; Neil et al., 2019). For each pixel, a set of weights defines how the different Chl-a algorithms are combined to determine an optimized Chl-a product. These weights are generally defined according to optical properties such as Chl-a (Smith et al., 2018) or the full reflectance spectra (Hieronymi et al., 2017; Neil et al., 2019). Such an approach has been tested in our dataset without success as it requires a stronger dataset with more data points and larger SPM, CDOM and Chl-a gradients. In the future, a refinement of the coarse weights (0,0.5,1) proposed here could be developed.

The QC tests presented in this paper were designed to maintain a relatively low uncertainty on the subset of data points where they apply. Their design was based on the relative difference between in situ and satellite estimates, which contrary to other statistical index such as RMSD allows to keep in situ Chl-a measurements as a reference. By creating the benefit function (Eq. (6)) we arbitrarily decide to retain data points with absolute percent difference less than 50% (positive score) and reject data points with more than 50% absolute percent difference (negative score). This limit has been chosen by analogy with oceanic water Chl-a applications (IOCCG report 18, 2019) and, in comparison to the average uncertainty measure in case 1 waters (35%, Hu et al., 2012; O'Reilly and Werdell, 2019). However, modification of this limit doesn't change dramatically the results as shown in Fig. S4 (supplementary material), as only $L_{logR5OC4}$ and $L_{logR5OC5}$ are slightly more restrictive when point selection becomes stricter. This shows that after a certain level it becomes difficult to keep reducing uncertainty by selecting best water type only. Indeed, other sources of uncertainty such as radiometric noise or uncertainty in atmospheric correction also impact Chl-a retrieval. Another approach avoiding not processed areas would be to provide a pixel-based uncertainty map (Moore et al., 2009; Hieronymi et al., 2017) allowing the user to set their own acceptable level of uncertainty. Although that would be more flexible and better fit to any type of application, producing high quality uncertainty estimates which vary with local water properties is still challenging and not systematically provided with Chl-a satellite products (IOCCG report 18, 2019). The QC tests presented here allow to easily identify reliable Chl-a pixels and ensure high quality Chl-a estimates in a robust but simple way.

4.3. Potential application for eutrophication monitoring

Eutrophication is the enrichment of water by nutrients causing an exponential development of primary producers (i.e. micro-algae and macro-algae). This environmental disturbance modifies the ecosystem balance and affects the quality of the waterbody (OSPAR, 2017). The eutrophication status is established by monitoring of nutrients and chlorophyll-a concentration as a proxy for phytoplankton biomass (Reinart and Kutser, 2006; Harvey et al., 2015). To ensure a good quality of marine waters, some national or multi-national policies requires a careful monitoring of coastal waters. For example, in the European Union, the objective of the Marine Strategy Framework Directive (MSFD) to reach a 'good environmental status' (GES) by 2020 (Gohin et al., 2008; Gohin et al., 2019; Gohin et al., 2020) is a key driver for monitoring the coastal and offshore waters in Europe. While in situ data acquisition is still considered as the main monitoring tool, the European Commission highlighted the need for greater coherence with related EU legislations (Water Framework Directive and Habitats and Birds Directive) and for more coherent and coordinated approaches within and between marine regions and sub-regions (European Commission, 2014). During recent years there has been a growing tendency to use optical remote sensing as a supporting tool to achieve the monitoring requirements because Chl-a satellite data combine cost-effective data collection with a much improved spatial and temporal coverage compared to in situ measurements. The satellite data also facilitates transnational spatial coherence which for MFSD monitoring avoids discrepancies between EU countries due to different in situ methodologies and protocols. The reliability of Chl-a estimates and the accurate assessment of uncertainty, which is important to users, is addressed by the methodology presented in this study. To test the relevance of this methodology in the framework of the MFSD eutrophication assessment, QC tests for OC4, OC5 and NIR-RED algorithms were applied in a North Sea wide eutrophication assessment and the merged Chl-a product was evaluated by a comparison analysis with in situ datasets for all assessment areas in the greater North Sea. The comparison of the yearly mean and P90 CHL products yielded a median difference of 35.19% and 39.05% (Van der Zande et al., 2019) validating the present methodology for eutrophication assessment in European waters.

For future applications, it has been shown that the direct application of the present methodology on OLCI data is straight forward because of the good match between OLCI and MERIS spectral bands. In addition, although a validation with in situ OLCI matchup is needed, the application of the present methodology on OLCI data (Fig. 14) shows coherent results. Regarding other optical sensors, there is an interest for coastal water monitoring to define QC tests for high resolution sensors such as Sentinel 2 – MSI or Landsat – 8, OLI. In that case, some adaptations are needed to account for spectral resolution of these sensors: (1) to use the CCRR-MERMAID database, band-shifts coefficients are needed, (2) some variables used in QC tests will need to be modified if the MERIS band doesn't exist in the high resolution sensor and (3) some Chl-a algorithms will have to be abandoned (i.e. OC5, NIR-RED with Landsat8-OLI) or adapted (OC4 to OC3) when spectral bands are missing.

5. Conclusion

Satellite data from ocean colour sensors (e.g., MERIS, Sentinel-3) can provide spatially coherent data for Chl-a. In coastal water, there is a high demand of reliable Chl-a images from end-users working for ecosystem management, fish and shell farming or eutrophication monitoring. However, because of the optical complexity of coastal waters as well as their high spatial and temporal variability, retrieving accurate Chl-a concentration remains challenging. In particular, if the study area is large or presents unknown or unpredictable water properties, the selection of the best Chl-a algorithm becomes very difficult. To help remote sensing users retrieving accurate Chl-a concentration, we presented QC tests for three popular Chl-a algorithms: OC4 (O'Reilly et al., 1998); OC5 (Gohin et al., 2002) and NIR-RED (Gons, 1999). These QC tests are built from a newly developed methodology directly based on the relative difference between Chl-a in situ measurements and simultaneous MERIS water reflectance. The simplicity of these tests which only require water reflectance data and provides a binary mask (i.e. Chl-a estimation from this algorithm is reliable or not) makes them easily accessible to the remote sensing user community. In addition, the combined utilization of these QC tests with the switching methodology allows to ensure a good coverage with 83% of our dataset processed. Although QC tests were designed from MERIS data and would need further validation with OLCI data, a comparison of MERIS and OLCI-A applications has shown very consistent patterns suggesting that present QC tests are also suitable to OLCI data. Thus, we expect that this methodology combined with OLCI data will help provide reliable monitoring of Chl-a in coastal waters for the coming decades, as needed for applications such as eutrophication management.

Declaration of Competing Interest

The authors declare that they have no known competing financial interests or personal relationships that could have appeared to influence the work reported in this paper.

Acknowledgements

This work has been funding by European Maritime and Fisheries Funds through DG ENV/MSFD Second Cycle/2016 Program (EUNOSAT project grant 11.0661/2017/750678/SUB/ENV.C2) and by the Swedish National Space Agency (Dnr. 175/17), ESA 21524/08/I-OL). It was also supported by funding from the European Union's Horizon 2020 Research and Innovation Programme grant agreement N 810139: Project Portugal Twinning for Innovation and Excellence in Marine Science and Earth Observation – PORTWIMS. We thank ESA/EUMETSAT/EU Copernicus for providing Sentinel-3 data and for permission to use them and ESA and ACRI-ST for developing ODESA and providing MEGS MERIS products (http://earth.eo.esa.int/odesa). ACRI-ST and ARGANS are acknowledged for the data processing and quality control on the MERMAID database. We also thank all the MERMAID contributors who provided in situ data:

- John Icely, UALG CIMA, Faro, Portugal
- Giuseppe Zibordi, Joint Research Centre of the European Commission, Ispra, Italy
- David Antoine, Curtin University, Perth, Western Australia
- David Mc Kee, Physics Dept, University of Strathclyde, Glasgow, Scotland
- Simon Bélanger, Université du Québec, Rimouski, Canada
- David A. Siegel, UC Santa Barbara, Santa Barbara, USA
- Catherine Belin, IFREMER, Brest, France

Three reviewers are acknowledged for very careful reading of the original text and many useful comments.

Appendix A. Supplementary data

Supplementary data to this article can be found online at https://doi.org/10.1016/j.rse.2020.112237.

References

Bailey, S., Werdell, P., 2006. A multi-sensor approach for the on-orbit validation of ocean color satellite data products. Remote Sens. Environ. 102 (1–2), 12–23. https://doi.org/10.1016/j.rse.2006.01.015.

Barker, K., Mazeran, C., Lerebourg, C., Bouvet, M., Antoine, D., Ondrusek, M., Zibordi, G., Lavender, S., 2008. Mermaid: the MERIS matchup in-situ database. In: Proceedings of the 2nd (A) ATSR and MERIS Workshop, Frascati, Italy.

Bricaud, A., Morel, A., 1987. Atmospheric corrections and interpretation of marine radiances in CZCS imagery: use of a reflectance model. Oceanol. Acta 7 (special issue), 33–50.

Bricaud, A., Morel, A., Babin, M., Allali, K., Claustre, H., 1998. Variations of light absorption by suspended particles with chlorophyll a concentration in oceanic (case 1) waters: analysis and implications for bio-optical models. J. Geophys. Res. 103 (C13), 31033–31044.

Camiolo, M.D., Cozzolino, E., Simionato, C.G., Hozbor, M.C., Lasta, C.Á., 2016. Evaluating the performance of the OC5 algorithm of IFREMER for the highly turbid waters of Río de la Plata. Braz. J. Oceanogr. 64 (1), 19–28.

Cardoso Dos Santos, J., Van Der Zande, D., Lavigne, H., 2019. Eutrophication Monitoring Based in a Multi-Algorithm Chlorophyll-a Product Using Sentinel-3 Data, Poster Presentation at Living Planet Symposium 13–17 May 2019, Milan, Italy.

Chassot, E., Bonhommeau, S., Dulvy, N.K., Mélin, F., Watson, R., Gascuel, D., Pape, O.L., 2010. Global marine primary production constrains fisheries catches. Ecol. Lett. 13 (4), 495–505. https://doi.org/10.1111/j.1461-0248.2010.01443.x.

Dall'Olmo, G., Gitelson, A.A., Rundquist, D.C., Leavitt, B., Barrow, T., Holz, J.C., 2005. Assessing the potential of SeaWiFS and MODIS for estimating chlorophyll concentration in turbid productive waters using red and near-infrared bands. Remote Sens. Environ. 96 (2), 176–187.

Dierssen, H.M., 2010. Perspectives on empirical approaches for ocean color remote sensing of chlorophyll in a changing climate. Proc. Natl. Acad. Sci. 107 (40), 17073–17078.

Doerffer, R., Schiller, H., 2007. The MERIS case 2 water algorithm. Int. J. Remote Sens. 28 (3–4), 517–535.

Druon, J.N., Schrimpf, W., Dobricic, S., Stips, A., 2004. Comparative assessment of large-scale marine eutrophication: North Sea area and Adriatic Sea as case studies. Mar. Ecol. Prog. Ser. 272, 1–23.

European Commission, 2014. The European Commission's Assessment and Guidance (COM/2014/097_final). Office for Official Publications of the European Communities, Luxembourg. https://eur-lex.europa.eu/legal-content/EN/TXT/?uri=celex%3A52014DC0097.

Fraysse, M., Pairaud, I., Ross, O.N., Faure, V.M., Pinazo, C., 2014. Intrusion of Rhone River diluted water into the Bay of Marseille: generation processes and impacts on ecosystem functioning. J. Geophys. Res. 119 (10), 6535–6556.

Garnesson, P., Mangin, A., d'Andon, O.F., Demaria, J., Bretagnon, M., 2019. The CMEMS GlobColour Chlorophyll-a Product Based on Satellite Observation. Ocean Science Discussions. https://doi.org/10.5194/os-2018-155.

Gernez, P., Doxaran, D., Barillé, L., 2017. Shellfish aquaculture from space: potential of Sentinel2 to monitor tide-driven changes in turbidity, chlorophyll concentration and oyster physiological response at the scale of an oyster farm. Front. Mar. Sci. 4, 137.

Gilerson, A.A., Gitelson, A.A., Zhou, J., Gurlin, D., Moses, W., Ioannou, I., Ahmed, S.A., 2010. Algorithms for remote estimation of chlorophyll-a in coastal and inland waters using red and near infrared bands. Opt. Express 18 (23), 24109–24125.

Gitelson, A., 1992. The peak near 700 nm on radiance spectra of algae and water: relationships of its magnitude and position with chlorophyll concentration. Int. J. Remote Sens. 13 (17), 3367–3373.

Gitelson, A.A., Schalles, J.F., Hladik, C.M., 2007. Remote chlorophyll-a retrieval in turbid, productive estuaries: Chesapeake Bay case study. Remote Sens. Environ. 109 (4), 464–472.

Gohin, F., 2011. Annual cycles of chlorophyll-a, non-algal suspended particulate matter, and turbidity observed from space and in-situ in coastal waters. Ocean Sci. 7 (5), 705–732. https://doi.org/10.5194/os-7-705-2011.

Gohin, F., Druon, J.N., Lampert, L., 2002. A five channel chlorophyll concentration algorithm applied to SeaWiFS data processed by SeaDAS in coastal waters. Int. J. Remote Sens. 23 (8), 1639–1661.

Gohin, F., Saulquin, B., Oger-Jeanneret, H., Lozac'h, L., Lampert, L., Lefebvre, A., Riou, P., Bruchon, F., 2008. Towards a better assessment of the ecological status of coastal waters using satellite-derived chlorophyll-a concentrations. Remote Sens. Environ. 112, 3329–3340. https://doi.org/10.1016/j.rse.2008.02.014.

Gohin, F., Van der Zande, D., Tilstone, G., Eleveld, M.A., Lefebvre, A., Andrieux-Loyer, F., Blauw, A.N., Bryère, P., Devreker, D., Garnesson, P., Hernández Fariñas, T., Lamaury, Y., Lampert, L., Lavigne, H., Menet-Nedelec, F., Pardo, S., Saulquin, S., 2019. 20 years of satellite and in situ observations of Chlorophyll-a from the northern Bay of Biscay to the eastern English Channel. Is the water quality improving? Remote Sens. Environ. 233, 111343 https://doi.org/10.1016/j.rse.2019.111343.

Gohin, F., Bryère, P., Lefebvre, A., Sauriau, P.G., Savoye, N., Vantrepotte, V., Courtay, G., 2020. Satellite and in situ monitoring of Chl-a, Turbidity, and total Suspended Matter in coastal waters: experience of the year 2017 along the French Coasts. J. Marine Sci. Eng. 8 (9), 665.

Gons, H.J., 1999. Optical teledetection of chlorophyll a in turbid inland waters. Environ. Sci. Technol. 33 (7), 1127–1132.

Gons, H.J., Rijkeboer, M., Ruddick, K.G., 2002. A chlorophyll-retrieval algorithm for satellite imagery (medium resolution imaging spectrometer) of inland and coastal waters. J. Plankton Res. 24 (9), 947–951.

Gons, H.J., Rijkeboer, M., Ruddick, K.G., 2005. Effect of a waveband shift on chlorophyll retrieval from MERIS imagery of inland and coastal waters. J. Plankton Res. 27 (1), 125–127.

Gons, H.J., Auer, M.T., Effler, S.W., 2008. MERIS satellite chlorophyll mapping of oligotrophic and eutrophic waters in the Laurentian Great Lakes. Remote Sens. Environ. 112 (11), 4098–4106.

Goyer, J., King, S., Borstad, G., Brown, L., 2005. Detection of intense plankton blooms using the 709 nm band of the MERIS imaging spectrometer. Int. J. Remote Sens. 26 (9), 2005–2012. https://doi.org/10.1080/01431160500075857.

Gurlin, D., Gitelson, A.A., Moses, W.J., 2011. Remote estimation of chl-a concentration in turbid productive waters—return to a simple two-band NIR-red model? Remote Sens. Environ. 115 (12), 3479–3490.

Harvey, E.T., Kratzer, S., Philipson, P., 2015. Satellite-based water quality monitoring for improved spatial and temporal retrieval of chlorophyll-a in coastal waters. Remote Sens. Environ. 158, 417–430. https://doi.org/10.1016/j.rse.2014.11.017.

Hieronymi, M., Müller, D., Doerffer, R., 2017. The OLCI Neural Network Swarm (ONNS): A bio-geo-optical algorithm for open ocean and coastal waters. Front. Mar. Sci. 4, 140.

Hu, C., Lee, Z., Franz, B., 2012. Chlorophyll algorithms for oligotrophic oceans: a novel approach based on three-band reflectance difference. J. Geophys. Res. 117 (C1).

IOCCG, 2019. Uncertainties in ocean colour remote sensing. In: Mélin, F. (Ed.), IOCCG Report Series, No. 18. International Ocean Colour Coordinating Group, Dartmouth, Canada. https://doi.org/10.25607/OBP-696.

Jackson, T., Sathyendranath, S., Mélin, F., 2017. An improved optical classification scheme for the ocean colour essential climate variable and its applications. Remote Sens. Environ. 203, 152–161. https://doi.org/10.1016/j.rse.2017.03.036.

Kahru, M., Mitchell, B.G., 2010. Blending of ocean colour algorithms applied to the Southern Ocean. Remote Sens. Lett. 1 (2), 119–124.

Katlane, R., Dupouy, C., Zargouni, F., 2012. Chlorophyll and Turbidity Concentrations Deduced From MODIS as an Index of Water Quality of the Gulf of Gabes in 2009. AUF. Télédétection 11, 1, CNRS & Campus Spatial Univ. Paris Diderot VII, pp. 265–273 (2012, Télédétection. hal-00746569).

Le, C., Li, Y., Zha, Y., Sun, D., Huang, C., Lu, H., 2009. A four-band semi-analytical model for estimating chlorophyll a in highly Turbid Lakes: the case of Taihu Lake, China. Remote Sens. Environ. 113 (6), 1175–1182.

Lee, Z., Hu, C., 2006. Global distribution of Case-1 waters: an analysis from SeaWiFS measurements. Remote Sens. Environ. 101 (2), 270–276.

Matsushita, B., Yang, W., Yu, G., Oyama, Y., Yoshimura, K., Fukushima, T., 2015. A hybrid algorithm for estimating the chlorophyll-a concentration across different trophic states in Asian inland waters. ISPRS J. Photogramm. Remote Sens. 102, 28–37.

Mélin, F., Vantrepotte, V., 2015. How optically diverse is the coastal ocean? Remote Sens. Environ. 160, 235–251.

Moore, T.S., Campbell, J.W., Feng, H., 2001. A fuzzy logic classification scheme for selecting and blending satellite ocean color algorithms. IEEE Trans. Geosci. Remote Sens. 39 (8), 1764–1776.

Moore, T.S., Campbell, J.W., Dowell, M.D., 2009. A class-based approach to characterizing and mapping the uncertainty of the MODIS Ocean chlorophyll product. Remote Sens. Environ. 113 (11), 2424–2430.

Morel, A., Bélanger, S., 2006. Improved detection of turbid waters from ocean color sensors information. Remote Sens. Environ. 102 (3–4), 237–249.

Morel, A., Prieur, L., 1977. Analysis of variations in ocean color. Limnol. Oceanogr. 22 (4), 709–722.

Moses, W.J., Gitelson, A.A., Berdnikov, S., Povazhnyy, V., 2009. Satellite estimation of chlorophyll-a concentration using the red and NIR bands of MERIS—the Azov Sea case study. IEEE Geosci. Remote Sens. Lett. 6 (4), 845–849.

Nechad, B., Ruddick, K., Schroeder, T., Oubelkheir, K., Blondeau-Patissier, D., Cherukuru, N., Brando, V., Dekker, A., Clementson, L., Banks, A.C., Maritorena, S., Werdell, J., Sá, C., Brotas, V., Caballero de Frutos, I., Ahn, Y.-H., Salama, S., Tilstone, G., Martinez-Vicente, V., Foley, D., McKibben, M., Nahorniak, J., Peterson, T., Siliò-Calzada, A., Röttgers, R., Lee, Z., Peters, M., Brockmann, C., 2015. CoastColour round Robin data sets: a database to evaluate the performance of algorithms for the retrieval of water quality parameters in coastal waters. Earth Syst. Sci. Data 7 (2), 319–348.

Neil, C., Spyrakos, E., Hunter, P.D., Tyler, A.N., 2019. A global approach for chlorophyll-a retrieval across optically complex inland waters based on optical water types. Remote Sens. Environ. 229, 159–178.

Nieke, J., Borde, F., Mavrocordatos, C., Berruti, B., Delclaud, Y., Riti, J.B., Garnier, T., 2012. The Ocean and Land Colour Imager (OLCI) for the Sentinel 3 GMES Mission: Status and First Test Results. In Earth Observing Missions and Sensors: Development, Implementation, and Characterization II, 8528. International Society for Optics and Photonics, p. 85280C.

Novoa, S., Chust, G., Sagarminaga, Y., Revilla, M., Borja, A., Franco, J., 2012. Water quality assessment using satellite-derived chlorophyll-a within the European directives, in the southeastern Bay of Biscay. Mar. Pollut. Bull. 64 (4), 739–750.

Odermatt, D., Gitelson, A., Brando, V.E., Schaepman, M., 2012. Review of constituent retrieval in optically deep and complex waters from satellite imagery. Remote Sens. Environ. 118, 116–126.

O'Reilly, J.E., Werdell, P.J., 2019. Chlorophyll algorithms for ocean color sensors-OC4, OC5 & OC6. Remote Sens. Environ. 229, 32–47.

O'Reilly, J.E., Maritorena, S., Mitchell, B.G., Siegel, D.A., Carder, K.L., Garver, S.A., Kahru, M., McClain, C., 1998. Ocean color chlorophyll algorithms for SeaWiFS. J. Geophys. Res. 103 (C11), 24937–24953.

OSPAR, 2017. Third OSPAR Integrated Report on the Eutrophication Status of the OSPAR Maritime Area (ISBN: 978-1-911458-34-0).

Park, Y.-J., Ruddick, K., Lacroix, G., 2010. Detection of algal blooms in European waters based on satellite chlorophyll data from MERIS and MODIS. Int. J. Remote Sens. 31 (24), 6567–6583.

Rast, M., Bezy, J.L., Bruzzi, S., 1999. The ESA medium resolution imaging spectrometer MERIS a review of the instrument and its mission. Int. J. Remote Sens. 20 (9), 1681–1702.

Reinart, A., Kutser, T., 2006. Comparison of different satellite sensors in detecting cyanobacterial bloom events in the Baltic Sea. Remote Sens. Environ. 102 (1), 74–85. https://doi.org/10.1016/j.rse.2006.02.013.

Ruddick, K.G., Gons, H.J., Rijkeboer, M., Tilstone, G., 2001. Optical remote sensing of chlorophyll a in case 2 waters by use of an adaptive two-band algorithm with optimal error properties. Appl. Opt. 40 (21), 3575–3585.

Sathyendranath, S., Prieur, L., Morel, A., 1989. A three-component model of ocean colour and its application to remote sensing of phytoplankton pigments in coastal waters. Int. J. Remote Sens. 10 (8), 1373–1394.

Smith, V.H., 2003. Eutrophication of freshwater and coastal marine ecosystems a global problem. Environ. Sci. Pollut. Res. 10 (2), 126–139. https://doi.org/10.1065/espr2002.12.142.

Smith, M.E., Robertson Lain, L., Bernard, S., 2018. An optimized chlorophyll a switching algorithm for MERIS and OLCI in phytoplankton-dominated waters. Remote Sens. Environ. 215, 217–227. https://doi.org/10.1016/j.rse.2018.06.002.

Steinmetz, F., Deschamps, P.-Y., Ramon, D., 2011. Atmospheric correction in presence of sun glint: application to MERIS. Opt. Express 19 (10), 9783–9800.

Tilstone, G.H., Angel-Benavides, I.M., Pradhan, Y., Shutler, J.D., Groom, S., Sathyendranath, S., 2011. An assessment of chlorophyll-a algorithms available for SeaWiFS in coastal and open areas of the Bay of Bengal and Arabian Sea. Remote Sens. Environ. 115 (9), 2277–2291.

Tilstone, G., Mallor-Hoya, S., Gohin, F., Couto, A.B., Sá, C., Goela, P., Cristina, S., Airs, R., Icely, J., Zühlke, M., 2017. Which ocean colour algorithm for MERIS in north west European waters? Remote Sens. Environ. 189, 132–151.

Van der Zande, D., Lavigne, H., Blauw, A., Prins, T., Desmit, X., Eleveld, M., Gohin, F., Pardo, S., Tilstone, G., Cardoso Dos Santos, J., 2019. Coherence in Assessment Framework of Chlorophyll A and Nutrients as Part of the EU Project 'Joint Monitoring Programme of the Eutrophication of the North Sea With Satellite Data' (Ref: DG ENV/MSFD Second Cycle/2016). Activity 2 Report (106 pp).

Volpe, G., Santoleri, R., Colella, V., Forneris, V., Brando, V., Garnesson, P., Taylor, B., Grant, M., 2019. Product User Manual for All Ocean Colour Products. COPERNICUS Marine Environment Monitoring Service.

Wang, M., Jiang, L., Son, S., Liu, X., Voss, K.J., 2020. Deriving consistent ocean biological and biogeochemical products from multiple satellite ocean color sensors. Opt. Express 28 (3), 2661–2682.

Zibordi, G., Mélin, F., Berthon, J.-F., Holben, B., Slutsker, I., Giles, D., D'Alimonte, D., Vandemark, D., Feng, H., Schuster, G., 2009. AERONET-OC: a network for the validation of ocean color primary products. J. Atmos. Ocean. Technol. 26 (8), 1634–1651.